# Assessing the relative impacts of satellite ozone and its precursor observations to improve global tropospheric ozone analysis using multiple chemical reanalysis systems

Takashi Sekiya[1], Emanuele Emili[2], Kazuyuki Miyazaki[3], Antje Inness[4], Zhen Qu[5], R. Bradley Pierce[6], Dylan Jones[7], Helen Worden[8], William Y.Y. Cheng[8], Vincent Huijnen[9], and Gerbrand Koren[10]

[1]Japan Agency for Marine-Earth Science and Technology, Yokohama 2360001, Japan
[2]Barcelona Supercomputing Center, Barcelona, Spain
[3]Jet Propulsion Laboratory/California Institute of Technology, Pasadena, CA, USA
[4]European Centre for Medium-range Weather Forecasts (ECMWF), Reading, UK
[5]Department of Marine Earth and Atmospheric Sciences, North Carolina State University, Raleigh, NC 27607, USA
[6]Space Science and Engineering Center, University of Wisconsin-Madison, Madison, WI 53706, USA
[7]Department of Physics, University of Toronto, Toronto, Ontario, Canada
[8]NSF National Center for Atmospheric Research, Boulder, CO, USA
[9]Royal Netherlands Meteorological Institute (KNMI), De Bilt, the Netherlands
[10]Copernicus Institute of Sustainable Development, Utrecht University, Utrecht, the Netherlands

**Correspondence:** Takashi Sekiya (tsekiya@jamstec.go.jp)

**Abstract.** Chemical reanalysis products have been produced by integrating various satellite observational data to provide comprehensive information on atmospheric composition. Five global chemical reanalysis datasets were used to evaluate the relative impacts of assimilating satellite ozone and its precursor measurements on surface and free tropospheric ozone analyses for the year 2010. Observing system experiments (OSEs) using the multiple reanalysis systems in similar settings were conducted to

5  examine the impacts of differences in reanalysis systems on observing system assessments. Without data assimilation, large discrepancies remained among the control runs owing to model biases. Data assimilation improved the consistency among the systems, reducing the standard deviation by 72–88% in the lower troposphere through the lower stratosphere, while improving agreement with independent ozonesonde observations. The OSEs suggested the importance of precursor measurements, especially from tropospheric $NO_2$ columns, for improving ozone analysis in the lower troposphere, with varying influences among

10  the systems (+0.1% in GEOS-Chem and +7% in TCR-2, with only $NO_2$ assimilation). Adjustments made by direct ozone assimilation showed similar vertical patterns between the TCR-2 and IASI-r systems, with increases of 6–22% and decreases of 2–21% in the middle and upper troposphere, respectively, reflecting the biases of the forecast models. These results suggest the importance of considering the effects of the forecast model performance and data assimilation configurations when assessing the observing system impacts to provide unbiased evaluations of satellite systems and to guide the design of future observing

15  systems.

## 1 Introduction

Tropospheric ozone plays a key role in climate systems as a short-lived climate forcer and in tropospheric photochemistry as a determinant of oxidizing capacity and methane lifetime (Szopa et al., 2021). It is also a hazardous air pollutant that adversely affects the human health, crop productivity, and ecosystems (Fleming et al., 2018; Mills et al., 2018). Tropospheric
20 ozone is chemically produced from precursor gases, including nitrogen oxides ($NO_x \approx NO + NO_2$), carbon monoxide (CO), and volatile organic compounds (VOCs), and it is destroyed through the chemical reaction of $O(^1D)$ with water vapor. Stratosphere–troposphere ozone exchange and dry deposition at the surface are also important ozone sources and sinks, respectively.

  The global tropospheric ozone distribution and its trends have been monitored in recent decades using various observation
25 networks, including surface in-situ networks, ozonesondes, ground-based remote sensing, aircrafts, and satellites (e.g., Schultz et al., 2017; Gaudel et al., 2018; Tarasick et al., 2019). In particular, a global picture of tropospheric ozone and its precursor gases has been provided from satellite observations, such as Global Ozone Monitoring Experiment (GOME) (Burrows et al., 1999), Measurements of Pollution in the Troposphere (MOPITT) (Drummond et al., 2010), Scanning Imaging Absorption SpectroMeter for Atmospheric Chartography (SCIAMACHY) (Callies et al., 2000), Ozone Monitoring Instrument (OMI)
30 (Levelt et al., 2006), Tropospheric Emission Spectrometer (TES) (Beer, 2006), and Microwave Limb Sounder (MLS) (Waters et al., 2006), GOME-2 (Callies et al., 2000), Infrared Atmospheric Sounding Interferometer (IASI) (August et al., 2012), and Tropospheric Monitoring Instrument (TROPOMI) (Veefkind et al., 2012). A recent study indicated that the complex impacts of various precursors on tropospheric ozone variability at regional to global scales depend on ozone chemical regimes and dynamical factors qualitatively, based on satellite and in-situ observations (Elshorbany et al., 2024). The combined use of
35 satellite observations of tropospheric ozone and its precursors remains a quantitative challenge because of the non-linear transport and chemistry processes involved with tropospheric ozone.

  Several chemical reanalysis products have been developed by integrating various observational datasets with chemical transport models using data assimilation techniques. These reanalysis products provide physically and chemically consistent long-term records of atmospheric composition, including tropospheric ozone. Chemical reanalysis products have been produced
40 using multi-species satellite observations, such as the Copernicus Atmosphere Monitoring Service (CAMS) reanalysis (CAMSRA) (Inness et al., 2019), the Tropospheric Chemistry Reanalysis version 2 (TCR-2) (Miyazaki et al., 2020a), and the Real-time Air Quality Modeling System (RAQMS) (Pierce et al., 2009). For CAMSRA and TCR-2, analyses of tropospheric ozone and related species have been validated using independent observations (Huijnen et al., 2020; Park et al., 2020; Ryu and Min, 2021). In experimental reanalysis, a smaller number of measurements are assimilated, such as tropospheric ozone in the IASI-r
45 (Emili and El Aabaribaoune, 2021) and tropospheric $NO_2$ in the GEOS-Chem-adjoint systems (Qu et al., 2020).

  The International Global Atmospheric Chemistry (IGAC) Tropospheric Ozone Assessment Report Phase II (TOAR-II) Chemical Reanalysis Focus Working Group (WG) summarizes the current status of chemical reanalysis to understand its capacity in various scientific applications. One of the important questions to be addressed is the relative impacts of individual satellite observations of stratospheric and tropospheric ozone and its precursors on surface and free tropospheric ozone anal-

50 yses. Resolving this question is essential for formulating future satellite missions and comprehending our understanding of the atmospheric chemistry and climate systems. Observing system experiments (OSEs), that separately assimilate individual measurements, have been widely used in meteorological studies to optimize the data assimilation frameworks, and they have contributed to the observing system development. In atmospheric composition research, the individual impacts of satellite observations of tropospheric ozone and its precursor gases (e.g., $NO_2$ and CO) have been evaluated using data assimilation and

55 chemical reanalysis frameworks (e.g., Barré et al., 2015; Miyazaki et al., 2019; Zhang et al., 2019; Emili and El Aabaribaoune, 2021; Inness et al., 2022; Naus et al., 2022; Sekiya et al., 2022).

Nevertheless, the implications of OSE results can be strongly affected by the the forecast model performance because of the perfect model assumption. They are also influenced by the data assimilation configurations, such as the data assimilation technique and choice of data version or satellite product level. Model-independent implications can be obtained using multi-

60 model approaches in a common OSE framework. In a pioneering study of multi-model chemical data assimilation, Miyazaki et al. (2020b) assessed the combined impacts of assimilating multi-constituent observations into multiple models using the Multi-mOdel Multi-cOnstituent Chemical data assimilation (MOMO-Chem) framework and showed strong model dependence on emission estimates and model response to the posteriori emissions. Similarly, OSEs using a variety of chemical reanalysis systems allow for observational impact assessments that are less dependent on the characteristics of individual forecast models

65 and data assimilation systems. Such OSE results can support the developments of chemical reanalysis and future satellite missions.

Therefore, based on the work of the IGAC TOAR-II Chemical Reanalysis WG activity, this study utilized five global chemical reanalysis systems, CAMSRA, TCR-2, IASI-r, GEOS-Chem, and RAQMS, to evaluate the combined and individual impacts of assimilating multiple satellite observations on tropospheric ozone analysis. Although the assimilated measurements varied

70 between the reanalysis systems, we performed additional OSEs in closer settings across the systems to examine the relative impacts of satellite ozone and precursor measurements and their dependence on reanalysis systems.

The remainder of this paper is organized as follows. Section 2 describes the considered chemical reanalysis data and independent observational data for the validation. Section 3 compares the five chemical reanalysis products and validates them using independent observations. Section 4 presents the assessment results on the impacts of assimilating individual observa-

75 tions on tropospheric ozone analysis. Section 5 discusses future chemical reanalysis developments and satellite constellation designs. Section 6 summarizes this study.

## 2 Data

### 2.1 Reanalysis systems

Table 1 summarizes the chemical reanalysis products used in this study. Data assimilation calculations and validations were

80 conducted for 2010, because a greater number of satellite observations were available compared with other years. Brief descriptions of these systems are provided as below.

### 2.1.1 CAMS reanalysis (CAMSRA)

CAMS (Peuch et al., 2022), operated by the European Centre for Medium-Range Weather Forecasts (ECMWF) on behalf of the European Commission, provides daily analyses and 5-day forecasts of atmospheric composition in near-real time as
85 well as a reanalysis of atmospheric composition going back to 2003, known as the CAMSRA (Inness et al., 2019). CAMSRA consists of three-dimensional time-consistent atmospheric composition fields, including aerosols and chemical species. It builds on the experience gained during the production of the earlier Monitoring Atmospheric Composition and Climate (MACC) reanalysis (Inness et al., 2013) and CAMS interim reanalysis (Flemming et al., 2017). Satellite retrievals of the total column CO, tropospheric column $NO_2$, aerosol optical depth, and ozone ($O_3$) were assimilated for CAMSRA with ECMWF's Integrated
90 Forecasting System. The $O_3$ retrievals assimilated in CAMSRA were total column fields from SCIAMACHY, OMI, GOME-2 and TROPOMI, ozone layers from SBUV/2, and ozone profiles from MIPAS and MLS. Offline or reprocessed retrievals were used until 2016 and near-real time retrievals were used from 2017 onwards. More details can be found in Inness et al. (2019) and in the reanalysis validation reports available at https://atmosphere.copernicus.eu/eqa-reports-global-services.

CAMSRA has a horizontal resolution of about 80 km and provides 3-hourly 3D analysis fields and forecast fields, 3-hourly
95 forecast fields as well as hourly surface forecast fields. It was produced with ECMWF's incremental 4-dimensional variational (4D-Var) data assimilation system (Courtier et al., 1994), with 12-hour assimilation windows from 09 UTC to 21 UTC and 21 UTC to 09 UTC and two minimisations at spectral truncations T95 (~210 km) and T159 (~110 km). Several atmospheric composition fields (i.e. $O_3$, CO, $NO_2$ and total aerosol mass mixing ratio) were included in the control vector and minimized together with the meteorological control variables, by adjusting the initial conditions. Emissions were not optimised. The
100 background errors for $O_3$ were calculated with the National Meteorological Center (NMC) method (Parrish and Derber, 1992) and are univariate; i.e. the error covariance matrix between ozone and the other chemical and dynamical fields is diagonal.

The chemical mechanism of the IFS used in CAMSRA was a modified and extended version of the CB05 (Yarwood et al., 2005) chemical mechanism for the troposphere, as implemented in the chemical transport model (CTM) TM5 (Huijnen et al., 2010). CB05 describes the tropospheric chemistry with 55 species and 126 reactions. Stratospheric ozone chemistry was
105 parameterized by a "Cariolle-scheme" (Cariolle and Déqué, 1986; Cariolle and Teyssèdre, 2007). Ozone and aerosol fields were used interactively in the numerical weather prediction (NWP) radiation scheme of CAMSRA.

The anthropogenic emissions used in CAMSRA came from the MACCity inventory (Granier et al., 2011), with modifications to increase winter-time road traffic emissions over North America and Europe following the correction of Stein et al. (2014). Biomass burning emissions were taken from the Global Fire Assimilation System (GFAS v1.2; Kaiser et al., 2012). Monthly
110 mean biogenic emissions simulated by the MEGAN2.1 model following Sindelarova et al. (2014) were used for the period 2003–2017, and in the later years a monthly-mean climatology derived from the 2003–2017 simulations was applied.

The validation in Inness et al. (2019) showed that the CAMSRA has smaller biases compared with observations than the previous two reanalyses (MACC and CAMS interim) and is more consistent in time, especially compared to the MACC reanalysis (e.g., Inness et al., 2019; Wagner et al., 2021). Evaluation of more recent years can be found in the validation reports

115 at https://atmosphere.copernicus.eu/eqa-reports-global-services. In addition to CAMSRA, CAMS also produced a control run which used the same meteorology as CAMSRA but did not assimilate any atmospheric composition data.

### 2.1.2 TCR-2

The TCR-2 products (Miyazaki et al., 2020a) were obtained from the assimilation of the OMI, SCIAMACHY, GOME-2 $NO_2$ QA4ECV v1.1 products (Boersma et al., 2017a, b, c), the TES V6 ozone profile, the MLS v4.2 ozone and $HNO_3$ (Livesey

120 et al., 2018), the MOPITT $CO$ v7 TIR/NIR product (Deeter et al., 2017), and the OMI PBL $SO_2$ product (Li et al., 2013). The reanalysis calculation was conducted at a horizontal resolution of T106 ($\sim$1.1°$\times$1.1°) with 32 vertical layers up to an altitude of 40 km using the MIROC-Chem global chemical transport model (Sekiya et al., 2018) and an ensemble Kalman filter (EnKF) technique.

The forecast model calculates tracer transport, emissions, deposition, and chemical processes, including the ozone-$HO_x$-

125 $NO_x$-CO-VOCs system (92 chemical species and 262 chemical reactions). The meteorological fields calculated in the dynamical and physical modules of MIROC-Chem were nudged to the 6-hourly ERA-Interim reanalysis (Dee et al., 2011) and used in the chemical module at every model time step (4–8 min).

The TCR-2 reanalysis system employs the local ensemble transform Kalman filter (LETKF) technique (Hunt et al., 2007). The state vector includes the surface emissions of $NO_x$, CO, and $SO_2$, and lightning $NO_x$ sources, as well as the concentrations

130 of 35 chemical species. Surface and lightning emissions were estimated based on a state argumentation method (e.g., Evensen, 2009), which used the relationship between emissions and concentrations in the background error covariance matrix generated based on ensemble model simulations. In the analysis step, the standard deviation of the emission ensembles was inflated to a predefined minimum value obtained through sensitivity calculations (i.e., 56% of the a priori emissions) to prevent covariance underestimation.

135 A priori emissions were obtained from the HTAP v2.2 inventory for the anthropogenic sources (Janssens-Maenhout et al., 2015) and the GFED v4.1 inventory for the biomass burning (Randerson et al., 2018), while those from soil $NO_x$ were based on the GEIA inventory (Graedel et al., 1993).

A control model simulation without any data assimilation, which was evaluated by Miyazaki et al. (2020a), was used as the baseline in this study.

140 ### 2.1.3 IASI-r

IASI-r (Emili and El Aabaribaoune, 2021) is a year long reanalysis experiment conceived to demonstrate the added value of assimilating ozone sensitive infrared measurements from the Infrared Atmospheric Sounding Interferometer (August et al., 2012). It was prepared based on previous experience in assimilating IASI Level 2 ozone retrievals (Emili et al., 2014; Peiro et al., 2018) and Level 1 radiances (Emili et al., 2019; Aabaribaoune et al., 2021).

145 The chemical transport model being used was MOCAGE (Josse et al., 2004), and it was setup on a 2x2 degrees global grid with 60 vertical levels up to 0.1 hPa and using meteorological forcing from ERA-interim (Dee et al., 2011). The IASI-r configuration employs a linearized ozone chemistry thorough the entire atmosphere (Cariolle and Teyssèdre, 2007), with the

ozone in the middle and lower troposphere being relaxed to a static zonal climatology. This relatively light model configuration is meant to run long term ozone reanalyses (Peiro et al., 2018), with assimilated observations providing the main spatio-temporal constraint on tropospheric ozone distribution.

IASI-r assimilates both ozone-sensitive radiances (Level 1) from IASI (980-1100 cm$^{-1}$) and stratospheric level 2 profiles from the Microwave Limb Sounder (MLS) using a 3-dimensional variational (3D-Var) data assimilation algorithm and hourly windows. Background and observation error covariances were either diagnosed (Aabaribaoune et al., 2021) or specified as a function of the vertical layer, tropopause height, and local ozone concentration (Emili and El Aabaribaoune, 2021). With the given setup, only ozone concentrations can be corrected by the data assimilation. Due to the limited vertical sensitivity of the assimilated observations and the simplified model configuration, little information is provided by IASI-r on ground-level ozone. Hence, the main target of IASI-r is ozone in the free and upper troposphere.

### 2.1.4 GEOS-Chem

We used the GEOS-Chem adjoint model (Henze et al., 2007) v35k to assimilate tropospheric $NO_2$ observations from OMI and simulate global ozone concentrations using the posterior $NO_x$ emissions at the $2° \times 2.5°$ resolution for 2005–2016. The GEOS-Chem model is driven by the Modern-Era Retrospective analysis for Research and Applications, Version 2 (MERRA-2) meteorological fields from the NASA Global Modeling and Assimilation Office (GMAO). Prior anthropogenic emissions of $NO_x$, $SO_2$, $NH_3$, CO, NMVOCs (non-methane volatile organic compounds), and primary aerosols were obtained from the HTAP 2010 inventory version 2 (Janssens-Maenhout et al., 2015). We also obtained 3-hourly wildfire emissions from GFED4 (Giglio et al., 2013). The other emissions and setups follow those of Qu et al. (2017, 2019a, b, 2020).

The OMI Level 2 $NO_2$ retrieval from the NASA product OMNO2 version 3 (Krotkov et al., 2017) was used for the assimilation. We screened all OMI $NO_2$ retrievals using data quality flags and by the criteria of positive tropospheric column, cloud fraction of $< 0.2$, solar zenith angle $< 75°$, and viewing zenith angle of $< 65°$. All retrievals that are affected by row anomalies were excluded. GEOS-Chem $NO_2$ vertical column densities (VCDs) were converted to slant column densities (SCDs) using scattering weight from the OMI retrievals and then compared the GEOS-Chem SCDs with the SCDs retrieved from OMI. A cost function was defined as the observation-error-weighted differences between the simulated and retrieved $NO_2$ SCDs plus the prior emissions error-weighted departure of the emission scaling factors from the prior estimates. The GEOS-Chem adjoint model minimizes the cost function using the quasi-Newton L-BFGS-B gradient-based optimization technique (Byrd et al., 1995; Zhu et al., 1994), in which the gradient of the cost function with respect to the control parameter is calculated using the adjoint method. Details of the assimilation of $NO_2$ SCDs, how vertical sensitivities of satellite retrievals are accounted for, and the hybrid 4D-Var/mass balance inversion of $NO_x$ emissions are described in Qu et al. (2017).

### 2.1.5 RAQMS

The RAQMS chemical reanalysis uses satellite trace gas and aerosol retrievals from the NASA satellites (Terra, Aqua, and Aura) covering 2006 through 2016. The operational grid point statistical interpolation (GSI) 3d variational analysis system (Wu et al., 2002) was used to assimilate retrievals from the Aura Ozone Monitoring Instrument (OMI) cloud cleared total

column ozone (McPeters et al., 2008), Microwave Limb Sounder (MLS) (Froidevaux et al., 2008) stratospheric ozone profiles, OMI tropospheric column $NO_2$ (Boersma et al., 2007), Terra and Aqua Moderate Resolution Imaging Spectrometer (MODIS) aerosol optical depth (AOD) (Remer et al., 2005), and Atmospheric Infrared Sounder (AIRS) carbon monoxide (Yurganov et al., 2008) at three-hour intervals. Analysis increments from the OMI tropospheric column $NO_2$ assimilation were used for off-line

185   adjustment of the a priori 2010 Hemispheric Transport of Air Pollution (HTAP, 2010) anthropogenic emission inventories following an offline mass balance approach similar to East et al. (2022). RAQMS biomass burning emissions used Terra and Aqua MODIS fire detections following Soja et al. (2004). The dynamical core of RAQMS is the UW-Hybrid model (Schaack et al., 2004). RAQMS-Aura meteorological predictions were initialized at 6-hour intervals with archived analyses from the National Center for Environmental Prediction (NCEP) Global Data Assimilation System (GDAS) (Kleist et al., 2009).

190   **2.2   Observing system experiments (OSEs)**

The assimilated measurements were largely different among the systems, which increased the difficultiy of implementing common OSE settings. The categorization of the assimilated measurements can be simplified into the three groups: stratospheric ozone (S), including total ozone column retrievals derived from backscatter ultraviolet (UV) instruments and ozone profile retrievals using microwave instruments; tropospheric ozone (T), consisting of ozone profiles obtained from infrared

195   (IR) instruments; and ozone precursors (P), including tropospheric $NO_2$ column retrievals from UV/visible sensors and total CO column and profile retrievals derived from IR instruments. As summarized in Table 2, five chemical reanalysis datasets and additional OSEs were divided into the following three types: (1) simultaneous assimilation of ozone and its precursors (S+T+P and S+P), (2) direct ozone assimilation (S+T, S, and T), and (3) assimilation of ozone precursor gases such as $NO_2$ and CO (P). We also performed OSEs using the TCR-2 and IASI-r chemical reanalysis systems, including four TCR-2 OSEs

200   that assimilated MLS stratospheric ozone and $HNO_3$ profiles (hereinafter TCR-2-S, type 2), TES tropospheric ozone profile (TCR-2-T, type 2), OMI, SCIAMACHY, and GOME-2 $NO_2$ (TCR-2-P_$NO_2$, type 3), and MOPITT CO (TCR-2-P_CO, type 3); and an IASI-r OSE for the IASI L1 radiance sensitive to tropospheric ozone profile (IASI-r-T, type 2).

**2.3   Validation data**

**2.3.1   OMI-MLS satellite observations**

205   For the validation, we used global distributions of the tropospheric ozone column (TOC) derived from OMI-MLS (Ziemke et al., 2006), which is a relatively independent data product that was not used in three of the chemical reanalysis systems (but both OMI total ozone column and MLS ozone profiles were assimilated in CAMSRA and RAQMS). The TOC from OMI-MLS was produced using the tropospheric ozone residual method, which subtracted the MLS stratospheric ozone column from the OMI total ozone column. The OMI-MLS TOC was derived using tropopause pressure determined from NCEP analyses with

210   the $2 \, \text{K} \, \text{km}^{-1}$ vertical temperature gradient criterion of the World Meteorological Organization (WMO). The $1\sigma$ precision for the monthly-mean TOC was estimated to be approximately 1.3 DU (Ziemke et al., 2019). For comparison with the OMI-MLS TOC, the same tropopause data from NCEP analyses were applied to the chemical reanalysis products.

### 2.3.2 Ozonesonde observations

The vertical profiles of the ozone analyses were validated against independent ozonesonde observations obtained from the
215 World Ozone and Ultraviolet Data Center (WOUDC; http://www.woudc.org). The measurement precision was better than 5%,
and the accuracy was within 5–10% (Smit et al., 2007). We used 261 profiles for the northern high latitudes (60–90°N), 1284
profiles for the northern mid-latitudes (30–60°N), 349 profiles for the tropics (30°N–30°N), 123 profiles for the southern mid-
latitudes (30–60°S), and 196 profiles for the southern high latitudes (60–90°S) from 2010. The observed and analyzed vertical
profiles were compared at ozonesonde locations in the 29 vertical pressure bins from 1013.25 to 70 hPa.

220 ### 2.3.3 Surface in situ observations

The TOAR global surface ozone database (Schultz et al., 2017) for 2010 was used to evaluate the surface ozone analyses. A
globally consistent TOAR database was constructed by combining almost 10,000 sites, characterizing the measurement sites,
and applying consistent quality control. The total uncertainty in modern ozone measurements (1990–2014) at a mean level
of 30 nmol mol$^{-1}$ was estimated at <2 nmol mol$^{-1}$ (Tarasick et al., 2019). The TOAR database provides annual, seasonal,
225 and monthly statistics for both urban and rural sites. All the reanalysis systems have relatively coarse horizontal resolutions;
therefore, they can not resolve ozone variability in urban areas. Thus, we used $2°\times2°$ monthly-mean ozone concentrations at
the rural sites in 2010. For the comparison, all the ozone analysis fields were regridded from the original grid points onto a
$2°\times2°$ grid.

## 3 Comparison of multiple chemical reanalysis products

230 ### 3.1 Data assimilation impacts

Figure 1 presents the vertical and latitudinal distributions of annual mean ozone concentrations obtained from the chemical
reanalysis products, control runs, and their differences for 2010. Large discrepancies in ozone concentrations between different
models were found in the lower stratosphere and troposphere, with the standard deviations of 27% in the global mean in the
upper troposphere and lower stratosphere (UTLS, 70–250 hPa), 8% in the middle troposphere (400–600 hPa), and 9% in the
235 lower troposphere (below 800 hPa).

Data assimilation increased the annual mean ozone concentrations in the UTLS in 2010 by 10–40% in CAMSRA and by
more than 100% in RAQMS, except in the tropics, and it decreased the concentrations by 5–30% in TCR-2 and IASI-r. In the
middle troposphere, data assimilation increased the global mean ozone in all the reanalysis products in most cases, with larger
increases in TCR-2, IASI-r, and RAQMS (by 15–50%) than in CAMSRA and GEOS-Chem (by up to 5%). This discrepancy
240 reflects the large inter-system differences in assimilation increments over the tropics. In the lower troposphere, data assimilation
increased the ozone concentration by 5–30% in CAMSRA, TCR-2, and RAQMS, whereas it only had minor impacts (< 5%) in
IASI-r and GEOS-Chem. Data assimilation also improved the consistency in ozone concentrations among the multiple systems,

with the standard deviation of the global mean ozone between different reanalysis systems reduced to 3.2% in the UTLS, 1.7%
in the middle troposphere, and 2.5% in the lower troposphere.

245    Similar reductions in the multi-model spread were observed for near-surface ozone (Fig. 2). The standard deviations of the
control runs were 22%, 11%, and 14% for the southern extratropics (25–90°S), the tropics (25°N–25°S), and the northern
extratropics (25–90°N), respectively. Data assimilation increased the near-surface annual mean ozone by 2–8 nmol mol$^{-1}$ in
CAMSRA, TCR-2, and RAQMS. The impact of assimilation on surface ozone was small in the IASI-r and GEOS-Chem. Data
assimilation reduced the standard deviation of ozone analyses between the reanalysis systems to 14%, 6%, and 11% over the
250    southern extratropics, tropics, and northern extratropics, respectively.

## 3.2    Validation using independent observations

### 3.2.1    OMI-MLS satellite observations

Figure 3 compares the tropospheric ozone column (TOC) between the chemical reanalysis products and control runs with OMI-
MLS TOC observations. All the control runs captured the observed general features. However, the CAMSRA and GEOS-Chem
255    control runs underestimated the TOC near 60°N and 60°S by up to 10 DU and overestimated the TOC from the tropics to the
subtropics in both hemispheres by 5–10 DU. In contrast, the TCR-2 control run overestimated the TOC over the northern
mid-latitudes by approximately 5 DU and the IASI-r control run overestimated the TOC over the southern mid-latitudes by
2–4 DU, whereas both models underestimated the TOC over the tropics and subtropics by 5–15 DU. The RAQMS control run
overestimated the TOC over the tropical land areas and the Atlantic by approximately 5 DU and underestimated the TOC over
260    the Pacific and the Southern Oceans by up to 10 DU. The spatial correlation coefficients of the observed vs. simulated TOC
ranged from 0.69 to 0.89.

After data assimilation, all the chemical reanalysis products commonly revealed positive biases of 5–10 DU from the tropics
to the mid-latitudes of both hemispheres. However, the spatial correlation coefficients were improved to > 0.83 in all the
systems. Thus, good consistency was observed among the reanalysis products. The remaining biases in the reanalysis products
265    indicate the difficulty of correcting tropospheric ozone through data assimilation of precursors and stratospheric profiles or
column measurements of ozone. This could be related to model errors near the surface (e.g., excessive chemical production
of ozone from precursors), differences in procedures for computing TOC between the observations and models (e.g., vertical
discretization around the tropopause), and positive biases of OMI-MLS against ozonesonde observations (Gaudel et al., 2024).
In the IASI-r and TCR-2 systems, tropospheric ozone profiles were assimilated. However, common positive biases against
270    OMI-MLS can partly be affected by positive biases in the assimilated tropospheric ozone retrievals (Boxe et al., 2010; Dufour
et al., 2012).

### 3.2.2    Ozonesondes

Figure 4 presents the vertical distributions of mean biases and root-mean-square errors (RMSEs) for the reanalysis products
and control runs relative to ozonesonde observations, over five latitude bands in 2010. As summarized in Table 3, in the UTLS

275 (70–250 hPa), large positive and negative ozone biases in the control runs varied among the models over all the latitude bands. The multi-model average RMSE against ozonesonde observations was 55±17% globally (44–61% for the five latitude bands).

In the middle troposphere (400–600 hPa), the model biases in the control runs were negative over the southern mid-latitudes and the northern mid-latitudes and high latitudes, whereas the biases varied among the models over the southern high latitudes and the tropics. The multi-model average RMSE was 28±4% (25–34% between the different latitude bands).

280 In the lower troposphere (800–900 hPa), model biases in the control runs differed between models over the southern mid-latitudes, high latitudes, and tropics, whereas the model biases were commonly negative over the northern mid-latitudes and high latitudes. The RMSE for ozone obtained from the multiple forecast models was 27±5% (20–43% over the five latitude bands).

Data assimilation reduced the mean biases in the UTLS to −3 to 9% over all the latitude bands relative to the control runs.
285 Over the tropics, the mean bias in TCR-2 was increased by 3% owing to data assimilation. Nevertheless, large positive and negative biases above and below 150 hPa were largely reduced by data assimilation, compared to the control runs in TCR-2. Data assimilation decreased the RMSEs of the multi-system mean and spread obtained from the reanalysis systems to 30±7% relative to global ozonesonde observations in the UTLS (18–40% over the five latitude bands).

In the middle troposphere, data assimilation increased the mean biases to 5–15% in TCR-2, IASI-r, and RAQMS over the
290 southern high latitudes relative to the control runs, although it decreased the mean biases in CAMSRA to less than 2%. Data assimilation also reduced the mean biases over the southern mid-latitudes (except for IASI-r), the tropics, and the northern mid-latitudes and high latitudes. The multi-system RMSE mean and spread were also decreased by data assimilation to 23±3%, compared to the control runs over the globe (21–28% over all the latitude bands).

In the lower troposphere, in contrast to the middle troposphere, the mean biases in TCR-2, IASI-r, and RAQMS were reduced
295 by up to 88% over the southern high latitudes, compared to the control runs, while the mean bias in CAMSRA was increased. Over the tropics, data assimilation increased the mean biases by 54% in TCR-2 and a factor of 4.4 in RAQMS. Over the southern mid-latitudes and northern mid-latitudes and high latitudes, data assimilation decreased the mean biases in all the reanalysis systems. The multi-system RMSE mean and spread were also reduced to 25±5% compared to global ozonesonde observations (18–42% over all the latitudes bands).

300 ### 3.2.3 Surface in situ networks

Figure 5 shows the model biases of the annual mean surface ozone against the TOAR database (Schultz et al., 2017) over the United States, Western Europe, and Northeast Asia for 2010. Over the United States, the control runs showed positive biases relative to the TOAR database, ranging from 2.4 to 16.2 nmol mol$^{-1}$. The spatial correlation coefficients and RMSEs in the control runs were 0.13–0.54 and 5.3–16.7 nmol mol$^{-1}$ compared to the TOAR database, respectively. After data assimilation,
305 the positive model biases were increased by up to a factor of 2.5. The spatial correlation coefficients were decreased by 0.01–0.05, except for TCR-2, whereas the RMSEs were increased by up to 31%.

Over Western Europe, surface ozone model biases in the control runs were 2.5–15.1 nmol mol$^{-1}$ relative to the TOAR database. The spatial correlation coefficients and RMSEs were 0.37–0.55 and 5.7–15.8 nmol mol$^{-1}$ compared to the TOAR

database, respectively. Data assimilation increased the positive model biases by a factor of up to two. The spatial correlation
310 coefficients were slightly decreased by 0.005–0.01 in CAMSRA and GEOS-Chem, whereas the spatial correlation coefficients
were increased by 0.02–0.06 in TCR-2 and RAQMS. The RMSEs were increased by 1–35%.

Over Northeast Asia, surface ozone model biases in the control runs were positive (4.2–17.8 nmol mol$^{-1}$) compared to
the TOAR database. The spatial correlation coefficients ranged from 0.01 to 0.5 among the models. The RMSEs against the
TOAR database were 7.6–18.8 nmol mol$^{-1}$. Through data assimilation, the model biases were increased by up to 42% in all
315 the systems. The spatial correlation coefficients were decreased by 0.03 in RAQMS but improved by 0.02–0.07 in CAMSRA,
TCR-2, and GEOS-Chem. The RMSEs were increased by up to 23% for all the systems.

Overall, the positive model bias of surface ozone against all available observations (0.3–12.8 nmol mol$^{-1}$) was increased by
data assimilation by up to a factor of 4. The spatial correlation coefficients were slightly decreased by data assimilation from
0.11–0.59 to 0.08–0.58, except for TCR-2. The RMSEs were increased by up to 18% for all the reanalysis products. Satellite
320 data assimilation reduced negative model biases in the free troposphere, whereas propagation of the ozone increments to the
surface increased surface ozone biases. These results indicate a misrepresentation of physical and chemical model processes
near the surface in the current global forecast models (Parrington et al., 2009; Travis et al., 2016) and highlight the need to
incorporate surface observations into the current global chemical reanalysis data (Hanea et al., 2004; Huang et al., 2013).

## 4 Relative impacts of satellite ozone and its precursor observations

325 ### 4.1 OSE results

OSEs were used to evaluate the relative impacts of individual assimilated measurements, as summarized in Table 2. In par-
ticular, we focused on three groups: (1) simultaneous assimilation of ozone and its precursors (S+T+P or S+P), (2) direct
assimilation of stratospheric and tropospheric ozone (S+T, S, or T), and (3) assimilation of ozone precursors including $NO_x$
and CO on ozone analysis (P($NO_2$) or P(CO)). As shown in Figs. 1, 2, 6, and 7, the effects of assimilation varied from system to
330 system. Nevertheless, similarities in the general patterns were observed. System-dependent differences in ozone increments can
be attributed to differences in model biases, data assimilation configurations (e.g., concentration and/or emission optimization),
and assimilated measurements.

For the simultaneous assimilation cases (S+T+P or S+P), in the UTLS, the global mean ozone concentrations increased
in CAMSRA (S+P) and RAQMS (S+P) by 18–61% but decreased in TCR-2 (S+T+P) by 21%. The discrepancy in the
335 increments reflects opposite model biases (c.f., Section 3.2.2). In the middle and lower troposphere, ozone concentrations
commonly increased over the extratropics but varied in magnitudes, ranging from 3% (CAMSRA) to 20% (TCR-2). Increases
in ozone near the surface were also common, with larger increases over remote areas than over the polluted and biomass-
burning areas. The increases in ozone concentrations obtained from the systems with emission optimization (by 11–27% in
TCR-2 and RAQMS) tended to be larger than those without optimization (by 4–11% in CAMSRA).
340 The direct ozone assimilation cases (S+T, S, or T) showed similar latitudinal and vertical patterns in the effects of data
assimilation in the middle to upper troposphere (Fig. 6), reflecting similar model biases in the MIROC-Chem and MOCAGE

models. The maximum changes in the tropical middle and lower troposphere was more than 40%. TCR-2-S (S), TCR-2-T (T), IASI-r (S+T), and IASI-r-T (T) increased the ozone concentration in the middle troposphere (by 6–22%) and decreased it in the UTLS (by 2–21%). Decreases in UTLS ozone in the assimilation of stratospheric ozone profiles (TCR-2-S (S) and IASI-r

345  (S+T)), were commonly larger than those in the assimilation of tropospheric ozone only (TCR-2-T (T) and IASI-r-T (T)). The effects on the tropical lower stratosphere and lower troposphere differed between TCR-2 and IASI-r. These different patterns may reflect differences in assimilated observations (TES vs. IASI) as well as model biases. Near the surface, direct ozone assimilation in TCR-2 showed large data assimilation impacts of up to 7%, 13%, and 8% in the southern extratropics, tropics, and northern extratropics, respectively (Fig. 7). The surface ozone change was smaller in IASI-r, partly because the prescribed

350  background error covariance (by 10%) in IASI-r in the lower troposphere was smaller than the ensemble spread of the ozone first guess (typically by 15–17%) in TCR-2. Other reasons for significant differences near the surface could be related to the altitude-dependent sensitivities of the assimilated observations (i.e., averaging kernels).

The assimilation of ozone precursor gases (P(NO$_2$) or P(CO)) increased the ozone concentrations in the lower and middle troposphere in the OSEs using TCR-2 and GEOS-Chem. The TCR-2 OSE results indicated a larger impact on the surface and

355  lower tropospheric ozone from the assimilation of NO$_2$ (by +7%) than from the assimilation of CO (by +1.5%). The impacts of tropospheric NO$_2$ assimilation varied among the systems, ranging from 0.1% (GEOS-Chem) to 7% (TCR-2). This discrepancy may be related to the smaller increments in NO$_x$ emissions in the GEOS-Chem adjoint calculation when assimilating the OMNO2 NASA standard product than those when assimilating the DOMINO and QA4ECV products (Qu et al., 2020). This discrepancy can also be caused by the different sensitivities of ozone to changing NO$_x$ emissions between GEOS-Chem and

360  MIROC-Chem (Miyazaki et al., 2020b) and the simultaneous corrections of NO$_x$ emissions and concentrations in TCR-2 (Miyazaki et al., 2012b). Meanwhile, the positive responses of ozone to MOPITT CO assimilation were consistently reported by Gaubert et al. (2016).

### 4.2   Validation against ozonesonde observations

As shown in Figs. 8 and 9, the chemical reanalysis products and OSEs were validated using ozonesonde observations. In the

365  extratropical UTLS, model biases were largely reduced by more than 67% by the simultaneous assimilation in CAMSRA (S+P), TCR-2 (S+T+P), and RAQMS (S+P). Over the tropics, model biases were also reduced by up to 74% in the lower stratosphere (70–150 hPa) and 44% in the upper troposphere (150–250 hPa), respectively (Fig. 9). The OSEs suggested the importance of the direct assimilation of stratospheric ozone profiles in IASI-r (S+T) and TCR-2-S (S), with bias reductions of 73–95% over the extratropics. Although the mean bias in the tropical UTLS (70–250 hPa) was increased in TCR-2-S, the

370  positive and negative biases were improved by 60% in the lower stratosphere and by 86% in the upper troposphere.

In the middle troposphere, the model bias was reduced by 88% in CAMSRA (S+P) over the southern high latitudes, whereas it was increased by 3–21% in TCR-2 (S+T+P) and RAQMS (S+P). Over the other four latitude bands, the simultaneous assimilation (S+T+P or S+P) improved the model biases compared to ozonesonde by 24–99%. The direct ozone assimilation of TES tropospheric ozone profile in TCR-2-T (T) showed bias reductions of 67% and 89% over the southern mid- and high

375  latitudes, respectively. In contrast, model biases were increased by the IASI tropospheric ozone assimilation in IASI-r (S+T).

Over the tropics, the model biases were reduced by 45–73% in TCR-2-T (T) and IASI-r (S+T) in the northern mid-latitudes and high latitudes. The assimilation of ozone precursor measurements in TCR-2-P_NOx and TCR-2-P_CO (P) reduced the model biases by 34–97% over all the latitude bands, with the exception of TCR-2-P_CO over the southern high latitudes.

In the lower troposphere, the simultaneous assimilation reduced the model biases over the southern high latitudes by up to 88% in TCR-2 (S+T+P) and RAQMS (S+P), except for CAMSRA (S+P). Over the tropics, the CAMSRA remained essentially unchanged (by 2%), whereas the other simultaneous assimilations increased model biases. Over the southern mid-latitudes, and northern mid-latitudes and high latitudes, all the simultaneous assimilation (S+T+P and S+P) reduced the negative model biases by 24–81%. Over the extratropics, the direct tropospheric ozone assimilation (S+T and T) reduced the model biases by up to 82%. Compared with these improvements, the assimilation of precursor measurements (P) showed comparable or larger bias reductions of 33–90% over the extratropics. Over the tropics, however, improvements in model biases were not found for the direct ozone assimilation or precursor assimilation (S+T, T, and P), except for IASI-r (by 59%). These results could partly be affected by biases in the assimilated measurements (Boxe et al., 2010), a lack of observational constraints on biogenic VOCs (De Smedt et al., 2018; Wells et al., 2022), and missing model processes, such as tropospheric halogen chemistry (Sherwen et al., 2016; Sekiya et al., 2020).

## 5  Discussion

The results obtained from multi-system OSEs have important implications for the development of a future satellite constellations. Multi-system OSE comparisons broadly suggested that integrating measurements of ozone and its precursors is an effective way to improve the entire profile of ozone in the troposphere and lower stratosphere. This has been commonly suggested by previous single-system OSE studies (e.g., Miyazaki et al., 2019), and indicates the great value of the current satellite constellation. Furthermore, the present study shows that the spread of data assimilation impacts among multiple systems can be used to evaluate whether the observing system impacts are dependent on the reanalysis system. These findings should lead to more robust assessments of the observing system impacts. The impact of assimilating OMI tropospheric $NO_2$ on lower tropospheric ozone varied from +0.1% to +7%. These results indicate that the assessment of observing system impacts is sensitive to the choice of data assimilation system. This difference reflects a variety of factors, including systematic biases among products derived from different retrieval algorithms (Qu et al., 2020), inappropriate data assimilation settings to fully exploit observational information (e.g., underestimation of background errors), and different model biases among systems.

However, even with improved observing systems, the impact of data assimilation will be limited because of the different complexities of chemical mechanisms (Huijnen et al., 2019; Miyazaki et al., 2020b), deposition processes (Hardacre et al., 2015; Young et al., 2018), and model physics, such as cloud formation and convective transport. Furthermore, VOCs such as formaldehyde (De Smedt et al., 2018) and isoprene (Wells et al., 2022) have not commonly been assimilated in the current chemical reanalysis systems. The lack of observations on important factors that determine chemical ozone formation underscores the need to fully exploit available observational information and causes underestimates of the value of the current observational system in the reanalysis framework.

Current chemical reanalysis systems employ various data assimilation techniques, including 3D-Var, 4D-Var, and EnKF.
410   These approaches differ in their assumptions and concepts and therefore in their performance (Lorenc and Rawlins, 2005; Kalnay et al., 2007). 4D-Var and EnKF exhibit comparable performance for both meteorological (Miyoshi et al., 2010) and chemical data assimilation (Wu et al., 2008; Skachko et al., 2014). A specific challenge in chemical data assimilation that differs from NWP is that chemical systems are stiff, stable, and highly dependent on input parameters, such as emissions and kinetic parameters (Carmichael et al., 2008; Miyazaki et al., 2012a). Therefore, the optimization of precursor emissions is considered
415   as an essential component of ozone analysis and OSE to provide a more meaningful evaluation of the current observing system. The feasibility and performance of emissions optimization using satellite observations, which have limited sensitivity to the lower troposphere, depends on data assimilation approaches. Nevertheless, optimizing precursor emissions using either online (i.e., simultaneous optimization of concentrations and emissions of various species) or offline (e.g., independent mass balance of a single species) approaches is important for improving the performance of OSE and reanalysis.

420   The OSEs presented in this study have important implications for improving the integration of future observations, including geostationary orbit (GEO) satellites and surface observations, in addition to low Earth orbit (LEO) satellites. The multi-system analysis suggested that the model bias at the surface is hardly reduced by the assimilation of any satellites. This highlights the importance of the data assimilation in surface observations (Kong et al., 2021) and machine learning (ML)-based bias corrections (He et al., 2022). However, obtaining sufficient global coverage for surface observing system remains a challenge.
425   The simultaneous assimilation of LEO and GEO satellites, such as GEMS, TEMPO, and Sentinel-4, is expected to improve our understanding of nonlinear ozone chemistry and its diurnal cycles at the urban scale across different regions. Moreover, such assimilation will allow us to estimate uncertain model parameters, such as diurnal emission profiles, kinetic reactions, and photolysis rates (Zoogman et al., 2014; Timmermans et al., 2019; Quesada-Ruiz et al., 2020; Shu et al., 2023). Advanced data assimilation techniques such as 4D-Var and EnKF are required to simultaneously and effectively assimilate observations from
430   different platforms.

## 6   Summary and conclusion

The IGAC TOAR-II Chemical Reanalysis WG activities summarized the capabilities of current chemical reanalysis products for various scientific applications. In this study, we evaluated the relative impacts of the assimilating satellite measurements of ozone and its precursors on surface and free tropospheric ozone analysis using five global chemical reanalysis systems, namely,
435   CAMSRA, TCR-2, IASI-r, GEOS-Chem, and RAQMS, for 2010. The use of multiple reanalysis systems allows for observing system impact assessments that are less dependent on the performance of individual forecast models and the configurations of individual data assimilation systems. Without data assimilation, large standard deviations in the ozone concentrations between the different models were found in the control runs. For example, the standard deviations were 27%, 8%, and 9% for UTLS, middle troposphere, and lower troposphere, respectively. Data assimilation improved the inter-system agreement and reduced
440   the standard deviation to 3.2%, 1.7%, and 2.5% for UTLS, middle troposphere, and lower troposphere, respectively. In most cases, the consistency with independent ozonesonde observations was also improved by data assimilation. The RMSEs against

global ozonesonde observations were reduced from 27 to 56% in the UTLS, middle troposphere, and lower troposphere to 23 to 30% by data assimilation. However, biases against surface in situ observations showed limited improvements after data assimilation in any of the reanalysis systems. This finding was probably because of the common positive biases of surface

445     ozone in global models (e.g., Turnock et al., 2020) and the low sensitivity of satellite observations to surface ozone.

Although the assimilated observations varied among the reanalysis systems, we examined the relative impacts of satellite ozone and precursor measurements and their dependence on reanalysis systems with additional OSEs in similar settings across some of the systems. These OSEs suggested the importance of including precursor measurements, especially for $NO_x$, to improve ozone analysis for the middle and lower troposphere. In addition, the impact of these measurements varied widely

450     between the systems, ranging from +0.1% (GEOS-Chem) to +7% (TCR-2). The impacts of direct ozone assimilation showed qualitatively similar latitudinal and vertical patterns between IASI-r and TCR-2, with increases by 6–22% and decreases by 2–21% in the middle troposphere and UTLS, respectively. The consistency with the ozonesonde observations was improved by the assimilation of ozone and its precursors, with bias reductions of up to 68% over the tropical middle troposphere and up to 89% over the middle troposphere over the northern mid-latitudes, respectively. The impacts of direct ozone assimilation were

455     dominant for the UTLS, with bias reductions of up to 91±9% over the northern mid-latitudes.

In conclusion, the simultaneous assimilation of satellite measurements of stratospheric and tropospheric ozone, and its precursors is an effective way to improve the overall tropospheric ozone analysis. The UTLS and middle tropospheric ozone analyses were consistently improved by satellite observations of the stratospheric and tropospheric ozone profiles, and the middle and lower tropospheric ozone analyses were also improved by the satellite observations of the ozone precursors. The

460     impacts of assimilating satellite observations on ozone analysis varied widely among the different reanalysis systems. Further investigation of the model dependence of the assimilating ozone precursor observations with more reanalysis systems is required to assess the uncertainties in the background error covariance between concentrations and emissions. These results indicate the importance of considering the effects of the forecast model performance and data assimilation configurations on the observing system impact assessments in order to provide an unbiased basis for the discussion of future observing system

465     designs.

*Data availability.* CAMS data are freely available from https://atmosphere.copernicus.eu/data. TCR-2 data can publicly be accessed at https://disc.gsfc.nasa.gov/information/data-release?title=Release%20of%20TROPESS%20Chemical%20Reanalysis%20Products. RAQMS chemical reanalysis data are archived at the University of Wisconsin-Madison Space Science and Engineering Center (SSEC) and can be made available upon request to R. B. Pierce, because. IASI-r data can be publicly accessed at https://b2share.cerfacs.fr/records/e3493962fb0e4e6b918d846b070de9d9.

470     GEOS-Chem-adjoint top-down $NO_x$ emission data are available at https://dataverse.harvard.edu/dataset.xhtml?persistentId=doi:10.7910/DVN/HVT1FO.

*Author contributions.* K.M., D.J., and H.W. designed the research. T.S., E.E., and W.C. performed the analysis. E.E., K.M., A.I., Z.Q., and B.P. provided chemical reanalysis products and OSE results. All the authors wrote and edited the paper manuscript.

*Competing interests.* The contact author has declared that neither they nor their co-authors have any competing interests.

*Acknowledgements.* The Copernicus Atmosphere Monitoring Service is operated by the European Centre for Medium-Range Weather Forecasts (ECMWF) on behalf of the European Commission as part of the Copernicus Programme (http://copernicus.eu). The TCR-2 product was generated by the calculations using the Earth Simulator with the support of the Japan Agency for Marine-Earth Science and Technology. Part of this work was conducted at the Jet Propulsion Laboratory, California Institute of Technology, under contract with the NASA. The RAQMS chemical reanalysis was supported by funding from the NASA Aura and Health and Air Quality (HAQ) Science Teams. We acknowledge the support of the National Aeronautics and Space Administration (NASA) Atmospheric Composition: Aura Science Team Program (19-AURAST19-0044), Atmospheric Composition Modeling and Analysis Program (22-ACMAP22-0013), NASA Earth Science U.S. Participating Investigator program (22-EUSPI22-0005). This work was also supported by the Environment Research and Technology Development Fund (JPMEERF20222001) of the Ministry of Environment of Japan and the JSPS KAKENHI grants (22K12353, 23H04971).

475

480

# References

485 Aabaribaoune, M. E., Emili, E., and Guidard, V.: Estimation of the error covariance matrix for IASI radiances and its impact on the assimilation of ozone in a chemistry transport model, Atmospheric Measurement Techniques, 14, 2841–2856, https://doi.org/10.5194/amt-14-2841-2021, 2021.

August, T., Klaes, D., Schlüssel, P., Hultberg, T., Crapeau, M., Arriaga, A., O'Carroll, A., Coppens, D., Munro, R., and Calbet, X.: IASI on Metop-A: Operational Level 2 retrievals after five years in orbit, J. Quant. Spectrosc. Radiat. Transf., 113, 1340–1371,
490 https://doi.org/10.1016/j.jqsrt.2012.02.028, 2012.

Barré, J., Gaubert, B., Arellano, A. F. J., Worden, H. M., Edwards, D. P., Deeter, M. N., Anderson, J. L., Raeder, K., Collins, N., Tilmes, S., Francis, G., Clerbaux, C., Emmons, L. K., Pfister, G. G., Coheur, P.-F., and Hurtmans, D.: Assessing the impacts of assimilating IASI and MOPITT CO retrievals using CESM-CAM-chem and DART, J. Geophys. Res., 120, 10,501–10,529, https://doi.org/10.1002/2015JD023467, 2015.

495 Beer, R.: TES on the aura mission: scientific objectives, measurements, and analysis overview, IEEE Trans. Geosci. Remote Sens., 44, 1102–1105, https://doi.org/10.1109/TGRS.2005.863716, 2006.

Boersma, K. F., Eskes, H. J., Veefkind, J. P., Brinksma, E. J., van der A, R. J., Sneep, M., van den Oord, G. H. J., Levelt, P. F., Stammes, P., Gleason, J. F., and Bucsela, E. J.: Near-real time retrieval of tropospheric $NO_2$ from OMI, Atmos. Chem. Phys, 7, 2103–2118, https://doi.org/10.5194/acp-7-2103-2007, 2007.

500 Boersma, K. F., Eskes, H., Richter, A., De Smedt, I, Lorente, A., Beirle, S., Van Geffen, J., Peters, E., Van Roozendael, M., and Wagner, T.: QA4ECV $NO_2$ tropospheric and stratospheric vertical column data from OMI (Version 1.1) [Data set], https://doi.org/10.21944/qa4ecv-no2-omi-v1.1, Royal Netherlands Meteorological Institute (KNMI), 2017a.

Boersma, K. F., Eskes, H., Richter, A., De Smedt, I., Lorente, A., Beirle, S., Van Geffen, J., Peters, E., Van Roozendael, M., and Wagner, T.: QA4ECV $NO_2$ tropospheric and stratospheric vertical column data from GOME-2A (Version 1.1) [Data set],
505 https://doi.org/10.21944/qa4ecv-no2-gome2a-v1.1, Royal Netherlands Meteorological Institute (KNMI), 2017b.

Boersma, K. F., Eskes, H., Richter, A., De Smedt, I., Lorente, A., Beirle, S., Van Geffen, J., Peters, E., Van Roozendael, M., and Wagner, T.: QA4ECV $NO_2$ tropospheric and stratospheric vertical column data from SCIAMACHY (Version 1.1) [Data set], https://doi.org/10.21944/qa4ecv-no2-scia-v1.1, Royal Netherlands Meteorological Institute (KNMI), 2017c.

Boxe, C. S., Worden, J. R., Bowman, K. W., Kulawik, S. S., Neu, J. L., Ford, W. C., Osterman, G. B., Herman, R. L., Eldering, A., Tarasick,
510 D. W., Thompson, A. M., Doughty, D. C., Hoffmann, M. R., and Oltmans, S. J.: Validation of northern latitude Tropospheric Emission Spectrometer stare ozone profiles with ARC-IONS sondes during ARCTAS: sensitivity, bias and error analysis, Atmos. Chem. Phys., 10, 9901–9914, https://doi.org/10.5194/acp-10-9901-2010, 2010.

Burrows, J. P., Weber, M., Buchwitz, M., Rozanov, V., Ladstätter-Weißenmayer, A., Richter, A., DeBeek, R., Hoogen, R., Bramstedt, K., Eichmann, K.-U., Eisinger, M., and Perner, D.: The Global Ozone Monitoring Experiment (GOME): Mission Concept and First Scientific
515 Results, J. Atmos. Sci., 56, 151–175, https://doi.org/10.1175/1520-0469(1999)056<0151:TGOMEG>2.0.CO;2, 1999.

Byrd, R. H., Lu, P., Nocedal, J., and Zhu, C.: A Limited Memory Algorithm for Bound Constrained Optimization, SIAM J. Sci. Comput., 16, 1190–1208, https://doi.org/10.1137/0916069, 1995.

Callies, J., Corpaccioli, E., Eisinger, M., Hahne, A., and Lefebvre, A.: GOME-2- MetOp's second-generation sensor for operational ozone monitoring, ESA bulletin, 102, 28–36, 2000.

520 Cariolle, D. and Déqué, M.: Southern hemisphere medium-scale waves and total ozone disturbances in a spectral general circulation model, J. Geophys. Res., 91, 10 825–10 846, https://doi.org/10.1029/JD091iD10p10825, 1986.

Cariolle, D. and Teyssèdre, H.: A revised linear ozone photochemistry parameterization for use in transport and general circulation models: multi-annual simulations, Atmos. Chem. Phys., 7, 2183–2196, https://doi.org/10.5194/acp-7-2183-2007, 2007.

Carmichael, G. R., Sandu, A., Chai, T., Daescu, D. N., Constantinescu, E. M., and Tang, Y.: Predicting air quality: Improvements through
525 advanced methods to integrate models and measurements, J. Comput. Phys., 227, 3540–3571, https://doi.org/10.1016/j.jcp.2007.02.024, 2008.

Courtier, P., Thépaut, J.-N., and Hollingsworth, A.: A strategy for operational implementation of 4D-Var, using an incremental approach, Q. J. R. Meteorol. Soc., 120, 1367–1387, https://doi.org/10.1002/qj.49712051912, 1994.

De Smedt, I., Theys, N., Yu, H., Danckaert, T., Lerot, C., Compernolle, S., Van Roozendael, M., Richter, A., Hilboll, A., Peters, E.,
530 Pedergnana, M., Loyola, D., Beirle, S., Wagner, T., Eskes, H., van Geffen, J., Boersma, K. F., and Veefkind, P.: Algorithm theoretical baseline for formaldehyde retrievals from S5P TROPOMI and from the QA4ECV project, Atmos. Meas. Tech., 11, 2395–2426, https://doi.org/10.5194/amt-11-2395-2018, 2018.

Dee, D. P., Uppala, S. M., Simmons, A. J., Berrisford, P., Poli, P., Kobayashi, S., Andrae, U., Balmaseda, M. A., Balsamo, G., Bauer, P., Bechtold, P., Beljaars, A. C. M., van de Berg, L., Bidlot, J., Bormann, N., Delsol, C., Dragani, R., Fuentes, M., Geer, A. J., Haimberger, L.,
535 Healy, S. B., Hersbach, H., Hólm, E. V., Isaksen, L., Kållberg, P., Köhler, M., Matricardi, M., McNally, A. P., Monge-Sanz, B. M., Morcrette, J.-J., Park, B.-K., Peubey, C., de Rosnay, P., Tavolato, C., Thépaut, J.-N., and Vitart, F.: The ERA-Interim reanalysis: configuration and performance of the data assimilation system, Q. J. R. Meteorol. Soc., 137, 553–597, https://doi.org/10.1002/qj.828, 2011.

Deeter, M. N., Edwards, D. P., Francis, G. L., Gille, J. C., Martínez-Alonso, S., Worden, H. M., and Sweeney, C.: A climate-scale satellite record for carbon monoxide: the MOPITT Version 7 product, Atmos. Meas. Tech., 10, 2533–2555, https://doi.org/10.5194/amt-10-2533-
540 2017, 2017.

Drummond, J. R., Zou, J., Nichitiu, F., Kar, J., Deschambaut, R., and Hackett, J.: A review of 9-year performance and operation of the MOPITT instrument, Adv. Space Res., 45, 760–774, https://doi.org/10.1016/j.asr.2009.11.019, 2010.

Dufour, G., Eremenko, M., Griesfeller, A., Barret, B., LeFlochmoën, E., Clerbaux, C., Hadji-Lazaro, J., Coheur, P.-F., and Hurtmans, D.: Validation of three different scientific ozone products retrieved from IASI spectra using ozonesondes, Atmos. Meas. Tech., 5, 611–630,
545 https://doi.org/10.5194/amt-5-611-2012, 2012.

East, J. D., Henderson, B. H., Napelenok, S. L., Koplitz, S. N., Sarwar, G., Gilliam, R., Lenzen, A., Tong, D. Q., Pierce, R. B., and Garcia-Menendez, F.: Inferring and evaluating satellite-based constraints on $NO_x$ emissions estimates in air quality simulations, Atmos. Chem. Phys., 22, 15 981–16 001, https://doi.org/10.5194/acp-22-15981-2022, 2022.

Elshorbany, Y., Ziemke, J., Strode, S., Petetin, H., Miyazaki, K., De Smedt, I., Pickering, K., Seguel, R., Worden, H., Emmerichs, T.,
550 Taraborrelli, D., Cazorla, M., Fadnavis, S., Buchholz, R., Gaubert, B., Rojas, N., Nogueira, T., Salameh, T., and Huang, M.: Tropospheric Ozone Precursors: Global and Regional Distributions, Trends and Variability, EGUsphere, 2024, 1–57, https://doi.org/10.5194/egusphere-2024-720, 2024.

Emili, E. and El Aabaribaoune, M.: Impact of Infrared Atmospheric Sounding Interferometer (IASI) thermal infrared measurements on global ozone reanalyses, Geosci. Model Dev., 14, 6291–6308, https://doi.org/10.5194/gmd-14-6291-2021, 2021.

555 Emili, E., Barret, B., Massart, S., Flochmoen, E. L., a. Piacentini, Amraoui, L. E., Pannekoucke, O., and Cariolle, D.: Combined assimilation of IASI and MLS observations to constrain tropospheric and stratospheric ozone in a global chemical transport model, Atmospheric Chemistry and Physics, 14, 177–198, https://doi.org/10.5194/acp-14-177-2014, 2014.

Emili, E., Barret, B., Flochmoën, E. L., and Cariolle, D.: Comparison between the assimilation of IASI Level 2 ozone retrievals and Level 1 radiances in a chemical transport model, Atmospheric Measurement Techniques, 12, 3963–3984, https://doi.org/10.5194/amt-12-3963-2019, 2019.

560    Evensen, G.: The ensemble Kalman filter for combined state and parameter estimation, IEEE Control Syst. Mag., 29, 83–104, 2009.

Fleming, Z. L., Doherty, R. M., von Schneidemesser, E., Malley, C. S., Cooper, O. R., Pinto, J. P., Colette, A., Xu, X., Simpson, D., Schultz, M. G., Lefohn, A. S., Hamad, S., Moolla, R., Solberg, S., and Feng, Z.: Tropospheric Ozone Assessment Report: Present-day ozone distribution and trends relevant to human health, Elem. Sci. Anth., 6, 12, https://doi.org/10.1525/elementa.273, 2018.

565    Flemming, J., Benedetti, A., Inness, A., Engelen, R. J., Jones, L., Huijnen, V., Remy, S., Parrington, M., Suttie, M., Bozzo, A., Peuch, V.-H., Akritidis, D., and Katragkou, E.: The CAMS interim Reanalysis of Carbon Monoxide, Ozone and Aerosol for 2003–2015, Atmos. Chem. Phys., 17, 1945–1983, https://doi.org/10.5194/acp-17-1945-2017, 2017.

Froidevaux, L., Jiang, Y. B., Lambert, A., Livesey, N. J., Read, W. G., Waters, J. W., Browell, E. V., and coauthors: Validation of Aura Microwave Limb Sounder Stratospheric Ozone Measurements, J. Geophys. Res., 113, https://doi.org/10.1029/2007JD008771, 2008.

570    Gaubert, B., Arellano Jr., A. F., Barré, J., Worden, H. M., Emmons, L. K., Tilmes, S., Buchholz, R. R., Vitt, F., Raeder, K., Collins, N., Anderson, J. L., Wiedinmyer, C., Martinez Alonso, S., Edwards, D. P., Andreae, M. O., Hannigan, J. W., Petri, C., Strong, K., and Jones, N.: Toward a chemical reanalysis in a coupled chemistry-climate model: An evaluation of MOPITT CO assimilation and its impact on tropospheric composition, J. Geophys. Res., 121, 7310–7343, https://doi.org/10.1002/2016JD024863, 2016.

Gaudel, A., Cooper, O. R., Ancellet, G., Barret, B., Boynard, A., Burrows, J. P., Clerbaux, C., Coheur, P.-F., Cuesta, J., Cuevas, E., Doniki,
575    S., Dufour, G., Ebojie, F., Foret, G., Garcia, O., Granados-Muñoz, M. J., Hannigan, J. W., Hase, F., Hassler, B., Huang, G., Hurtmans, D., Jaffe, D., Jones, N., Kalabokas, P., Kerridge, B., Kulawik, S., Latter, B., Leblanc, T., Le Flochmoën, E., Lin, W., Liu, J., Liu, X., Mahieu, E., McClure-Begley, A., Neu, J. L., Osman, M., Palm, M., Petetin, H., Petropavlovskikh, I., Querel, R., Rahpoe, N., Rozanov, A., Schultz, M. G., Schwab, J., Siddans, R., Smale, D., Steinbacher, M., Tanimoto, H., Tarasick, D. W., Thouret, V., Thompson, A. M., Trickl, T., Weatherhead, E., Wespes, C., Worden, H. M., Vigouroux, C., Xu, X., Zeng, G., and Ziemke, J.: Tropospheric Ozone Assessment Report:
580    Present-day distribution and trends of tropospheric ozone relevant to climate and global atmospheric chemistry model evaluation, Elem. Sci. Anth., 6, 39, https://doi.org/10.1525/elementa.291, 2018.

Gaudel, A., Bourgeois, I., Li, M., Chang, K.-L., Ziemke, J., Sauvage, B., Stauffer, R. M., Thompson, A. M., Kollonige, D. E., Smith, N., Hubert, D., Keppens, A., Cuesta, J., Heue, K.-P., Veefkind, P., Aikin, K., Peischl, J., Thompson, C. R., Ryerson, T. B., Frost, G. J., McDonald, B. C., and Cooper, O. R.: Tropical tropospheric ozone distribution and trends from in situ and satellite data, EGUsphere, 2024,
585    1–51, https://doi.org/10.5194/egusphere-2023-3095, 2024.

Giglio, L., Randerson, J. T., and van der Werf, G. R.: Analysis of daily, monthly, and annual burned area using the fourth-generation global fire emissions database (GFED4), J. Geophys. Res., 118, 317–328, https://doi.org/10.1002/jgrg.20042, 2013.

Graedel, T. E., Bates, T. S., Bouwman, A. F., Cunnold, D., Dignon, J., Fung, I., Jacob, D. J., Lamb, B. K., Logan, J. A., Marland, G., Middleton, P., Pacyna, J. M., Placet, M., and Veldt, C.: A compilation of inventories of emissions to the atmosphere, Global Biogeochem.
590    Cy., 7, 1–26, https://doi.org/10.1029/92GB02793, 1993.

Granier, C., Bessagnet, B., Bond, T., D'Angiola, A., Denier van der Gon, H., Frost, G. J., Heil, A., Kaiser, J. W., Kinne, S., Klimont, Z., Kloster, S., Lamarque, J.-F., Liousse, C., Masui, T., Meleux, F., Mieville, A., Ohara, T., Raut, J.-C., Riahi, K., Schultz, M. G., Smith, S. J., Thompson, A., van Aardenne, J., van der Werf, G. R., and van Vuuren, D. P.: Evolution of anthropogenic and biomass burning emissions of air pollutants at global and regional scales during the 1980–2010 period, Clim. Change, 109, 163, https://doi.org/10.1007/s10584-011-
595    0154-1, 2011.

Hanea, R. G., Velders, G. J. M., and Heemink, A.: Data assimilation of ground-level ozone in Europe with a Kalman filter and chemistry transport model, J. Geophys. Res., 109, https://doi.org/10.1029/2003JD004283, 2004.

Hardacre, C., Wild, O., and Emberson, L.: An evaluation of ozone dry deposition in global scale chemistry climate models, Atmos. Chem. Phys., 15, 6419–6436, https://doi.org/10.5194/acp-15-6419-2015, 2015.

600  He, T.-L., Jones, D. B. A., Miyazaki, K., Huang, B., Liu, Y., Jiang, Z., White, E. C., Worden, H. M., and Worden, J. R.: Deep Learning to Evaluate US $NO_x$ Emissions Using Surface Ozone Predictions, J. Geophys. Res., 127, e2021JD035 597, https://doi.org/10.1029/2021JD035597, 2022.

Henze, D. K., Hakami, A., and Seinfeld, J. H.: Development of the adjoint of GEOS-Chem, Atmos. Chem. Phys., 7, 2413–2433, https://doi.org/10.5194/acp-7-2413-2007, 2007.

605  Huang, M., Carmichael, G. R., Chai, T., Pierce, R. B., Oltmans, S. J., Jaffe, D. A., Bowman, K. W., Kaduwela, A., Cai, C., Spak, S. N., Weinheimer, A. J., Huey, L. G., and Diskin, G. S.: Impacts of transported background pollutants on summertime western US air quality: model evaluation, sensitivity analysis and data assimilation, Atmos. Chem. Phys., 13, 359–391, https://doi.org/10.5194/acp-13-359-2013, 2013.

Huijnen, V., Williams, J., van Weele, M., van Noije, T., Krol, M., Dentener, F., Segers, A., Houweling, S., Peters, W., de Laat, J., Boersma,
610  F., Bergamaschi, P., van Velthoven, P., Le Sager, P., Eskes, H., Alkemade, F., Scheele, R., Nédélec, P., and Pätz, H.-W.: The global chemistry transport model TM5: description and evaluation of the tropospheric chemistry version 3.0, Geosci. Model Dev., 3, 445–473, https://doi.org/10.5194/gmd-3-445-2010, 2010.

Huijnen, V., Pozzer, A., Arteta, J., Brasseur, G., Bouarar, I., Chabrillat, S., Christophe, Y., Doumbia, T., Flemming, J., Guth, J., Josse, B., Karydis, V. A., Marécal, V., and Pelletier, S.: Quantifying uncertainties due to chemistry modelling – evaluation of tropospheric
615  composition simulations in the CAMS model (cycle 43R1), Geosci. Model Dev., 12, 1725–1752, https://doi.org/10.5194/gmd-12-1725-2019, 2019.

Huijnen, V., Miyazaki, K., Flemming, J., Inness, A., Sekiya, T., and Schultz, M. G.: An intercomparison of tropospheric ozone reanalysis products from CAMS, CAMS interim, TCR-1, and TCR-2, Geosci. Model Dev., 13, 1513–1544, https://doi.org/10.5194/gmd-13-1513-2020, 2020.

620  Hunt, B. R., Kostelich, E. J., and Szunyogh, I.: Efficient data assimilation for spatiotemporal chaos: A local ensemble transform Kalman filter, Physica D, 230, 112–126, https://doi.org/10.1016/j.physd.2006.11.008, 2007.

Inness, A., Baier, F., Benedetti, A., Bouarar, I., Chabrillat, S., Clark, H., Clerbaux, C., Coheur, P., Engelen, R. J., Errera, Q., Flemming, J., George, M., Granier, C., Hadji-Lazaro, J., Huijnen, V., Hurtmans, D., Jones, L., Kaiser, J. W., Kapsomenakis, J., Lefever, K., Leitão, J., Razinger, M., Richter, A., Schultz, M. G., Simmons, A. J., Suttie, M., Stein, O., Thépaut, J.-N., Thouret, V., Vrekoussis, M., Zerefos,
625  C., and the MACC team: The MACC reanalysis: an 8 yr data set of atmospheric composition, Atmos. Chem. Phys., 13, 4073–4109, https://doi.org/10.5194/acp-13-4073-2013, 2013.

Inness, A., Ades, M., Agustí-Panareda, A., Barré, J., Benedictow, A., Blechschmidt, A.-M., Dominguez, J. J., Engelen, R., Eskes, H., Flemming, J., Huijnen, V., Jones, L., Kipling, Z., Massart, S., Parrington, M., Peuch, V.-H., Razinger, M., Remy, S., Schulz, M., and Suttie, M.: The CAMS reanalysis of atmospheric composition, Atmos. Chem. Phys., 19, 3515–3556, https://doi.org/10.5194/acp-19-3515-2019,
630  2019.

Inness, A., Aben, I., Ades, M., Borsdorff, T., Flemming, J., Jones, L., Landgraf, J., Langerock, B., Nedelec, P., Parrington, M., and Ribas, R.: Assimilation of S5P/TROPOMI carbon monoxide data with the global CAMS near-real-time system, Atmos. Chem. Phys., 22, 14 355–14 376, https://doi.org/10.5194/acp-22-14355-2022, 2022.

Janssens-Maenhout, G., Crippa, M., Guizzardi, D., Dentener, F., Muntean, M., Pouliot, G., Keating, T., Zhang, Q., Kurokawa, J., Wankmüller, R., Denier van der Gon, H., Kuenen, J. J. P., Klimont, Z., Frost, G., Darras, S., Koffi, B., and Li, M.: HTAP_v2.2: a mosaic of regional and global emission grid maps for 2008 and 2010 to study hemispheric transport of air pollution, Atmos. Chem. Phys., 15, 11 411–11 432, https://doi.org/10.5194/acp-15-11411-2015, 2015.

Josse, B., Simon, P., and Peuch, V.: Radon global simulations with the multiscale chemistry and transport model MOCAGE, Tellus B, 56, 339–356, https://doi.org/10.1111/j.1600-0889.2004.00112.x, 2004.

Kaiser, J. W., Heil, A., Andreae, M. O., Benedetti, A., Chubarova, N., Jones, L., Morcrette, J.-J., Razinger, M., Schultz, M. G., Suttie, M., and van der Werf, G. R.: Biomass burning emissions estimated with a global fire assimilation system based on observed fire radiative power, Biogeosciences, 9, 527–554, https://doi.org/10.5194/bg-9-527-2012, 2012.

Kalnay, E., Li, H., Miyoshi, T., Yang, S.-C., and Ballabrera-Poy, J.: 4-D-Var or ensemble Kalman filter?, Tellus A: Dyn. Meteorol. Oceanogr., 59, 758–773, https://doi.org/10.1111/j.1600-0870.2007.00261.x, 2007.

Kleist, D. T., Parrish, D. F., Derber, J. C., Treadon, R., Wu, W.-S., and Lord, S.: Introduction of the GSI into the NCEP Global Data Assimilation System, Weather and Forecasting, 24, 1691–1705, https://doi.org/10.1175/2009WAF2222201.1, 2009.

Kong, L., Tang, X., Zhu, J., Wang, Z., Li, J., Wu, H., Wu, Q., Chen, H., Zhu, L., Wang, W., Liu, B., Wang, Q., Chen, D., Pan, Y., Song, T., Li, F., Zheng, H., Jia, G., Lu, M., Wu, L., and Carmichael, G. R.: A 6-year-long (2013–2018) high-resolution air quality reanalysis dataset in China based on the assimilation of surface observations from CNEMC, Earth Syst. Sci. Data, 13, 529–570, https://doi.org/10.5194/essd-13-529-2021, 2021.

Krotkov, N. A., Lamsal, L. N., Celarier, E. A., Swartz, W. H., Marchenko, S. V., Bucsela, E. J., Chan, K. L., Wenig, M., and Zara, M.: The version 3 OMI $NO_2$ standard product, Atmos. Meas. Tech., 10, 3133–3149, https://doi.org/10.5194/amt-10-3133-2017, 2017.

Levelt, P., van den Oord, G., Dobber, M., Malkki, A., Visser, H., de Vries, J., Stammes, P., Lundell, J., and Saari, H.: The ozone monitoring instrument, IEEE Trans. Geosci. Remote Sens., 44, 1093–1101, https://doi.org/10.1109/TGRS.2006.872333, 2006.

Li, C., Joiner, J., Krotkov, N. A., and Bhartia, P. K.: A fast and sensitive new satellite $SO_2$ retrieval algorithm based on principal component analysis: Application to the ozone monitoring instrument, Geophys. Res. Lett., 40, 6314–6318, https://doi.org/10.1002/2013GL058134, 2013.

Livesey, N. J., Read, W. G., Wagner, P. A., Froidevaux, L., Lambert, A., Manney, G. L., Millán Valle, L. F., Pumphrey, H. C., Santee, M. L., Schwartz, M. J., Wang, S., Fuller, R. A., Jarnot, R. F., Knosp, B. W., Martinez, E., and Lay, R. R.: Aura Microwave Limb Sounder (MLS) Version 4.2x Level2 data quality and description document, Tech. rep., Jet Propul. Lab., Pasadena, CA, tech. Rep. JPL D33509 Rev. D, 2018.

Lorenc, A. C. and Rawlins, F.: Why does 4D-Var beat 3D-Var?, Q. J. R. Meteorol. Soc., 131, 3247–3257, https://doi.org/10.1256/qj.05.85, 2005.

McPeters, R., Kroon, M., Labow, G., Brinksma, E., Balis, D., Petropavlovskikh, I., Veefkind, J. P., Bhartia, P. K., , and Levelt, P. F.: Validation of the Aura Ozone Monitoring Instrument Total Column Ozone Product, J. Geophys. Res., 113, https://doi.org/10.1029/2007JD008802, 2008.

Mills, G., Pleijel, H., Malley, C. S., Sinha, B., Cooper, O. R., Schultz, M. G., Neufeld, H. S., Simpson, D., Sharps, K., Feng, Z., Gerosa, G., Harmens, H., Kobayashi, K., Saxena, P., Paoletti, E., Sinha, V., and Xu, X.: Tropospheric Ozone Assessment Report: Present-day tropospheric ozone distribution and trends relevant to vegetation, Elementa: Science of the Anthropocene, 6, 47, https://doi.org/10.1525/elementa.302, 2018.

Miyazaki, K., Eskes, H. J., and Sudo, K.: Global $NO_x$ emission estimates derived from an assimilation of OMI tropospheric $NO_2$ columns, Atmos. Chem. Phys., 12, 2263–2288, https://doi.org/10.5194/acp-12-2263-2012, 2012a.

Miyazaki, K., Eskes, H. J., Sudo, K., Takigawa, M., van Weele, M., and Boersma, K. F.: Simultaneous assimilation of satellite $NO_2$, $O_3$, CO, and $HNO_3$ data for the analysis of tropospheric chemical composition and emissions, Atmos. Chem. Phys., 12, 9545–9579, https://doi.org/10.5194/acp-12-9545-2012, 2012b.

Miyazaki, K., Sekiya, T., Fu, D., Bowman, K. W., Kulawik, S. S., Sudo, K., Walker, T., Kanaya, Y., Takigawa, M., Ogochi, K., Eskes, H., Boersma, K. F., Thompson, A. M., Gaubert, B., Barre, J., and Emmons, L. K.: Balance of Emission and Dynamical Controls on Ozone During the Korea-United States Air Quality Campaign From Multiconstituent Satellite Data Assimilation, J. Geophys. Res., 124, 387–413, https://doi.org/10.1029/2018JD028912, 2019.

Miyazaki, K., Bowman, K., Sekiya, T., Eskes, H., Boersma, F., Worden, H., Livesey, N., Payne, V. H., Sudo, K., Kanaya, Y., Takigawa, M., and Ogochi, K.: Updated tropospheric chemistry reanalysis and emission estimates, TCR-2, for 2005–2018, Earth Syst. Sci. Data, 12, 2223–2259, https://doi.org/10.5194/essd-12-2223-2020, 2020a.

Miyazaki, K., Bowman, K. W., Yumimoto, K., Walker, T., and Sudo, K.: Evaluation of a multi-model, multi-constituent assimilation framework for tropospheric chemical reanalysis, Atmos. Chem. Phys., 20, 931–967, https://doi.org/10.5194/acp-20-931-2020, 2020b.

Miyoshi, T., Sato, Y., and Kadowaki, T.: Ensemble Kalman Filter and 4D-Var Intercomparison with the Japanese Operational Global Analysis and Prediction System, Mon. Weather Rev., 138, 2846 – 2866, https://doi.org/10.1175/2010MWR3209.1, 2010.

Naus, S., Domingues, L. G., Krol, M., Luijkx, I. T., Gatti, L. V., Miller, J. B., Gloor, E., Basu, S., Correia, C., Koren, G., Worden, H. M., Flemming, J., Pétron, G., and Peters, W.: Sixteen years of MOPITT satellite data strongly constrain Amazon CO fire emissions, Atmospheric Chemistry and Physics, 22, 14 735–14 750, https://doi.org/10.5194/acp-22-14735-2022, 2022.

Park, S., Son, S.-W., Jung, M.-I., Park, J., and Park, S. S.: Evaluation of tropospheric ozone reanalyses with independent ozonesonde observations in East Asia, Geosci. Lett., 7, 12, https://doi.org/10.1186/s40562-020-00161-9, 2020.

Parrington, M., Jones, D. B. A., Bowman, K. W., Thompson, A. M., Tarasick, D. W., Merrill, J., Oltmans, S. J., Leblanc, T., Witte, J. C., and Millet, D. B.: Impact of the assimilation of ozone from the Tropospheric Emission Spectrometer on surface ozone across North America, Geophys. Res. Lett., 36, https://doi.org/10.1029/2008GL036935, 2009.

Parrish, D. F. and Derber, J. C.: The National Meteorological Center's Spectral Statistical-Interpolation Analysis System, Mon. Weather Rev., 120, 1747 – 1763, https://doi.org/10.1175/1520-0493(1992)120<1747:TNMCSS>2.0.CO;2, 1992.

Peiro, H., Emili, E., Cariolle, D., Barret, B., and Flochmoën, E. L.: Multi-year assimilation of IASI and MLS ozone retrievals: variability of tropospheric ozone over the tropics in response to ENSO, Atmospheric Chemistry and Physics, 18, 6939–6958, https://doi.org/10.5194/acp-18-6939-2018, 2018.

Peuch, V.-H., Engelen, R., Rixen, M., Dee, D., Flemming, J., Suttie, M., Ades, M., Agustí-Panareda, A., Ananasso, C., Andersson, E., Armstrong, D., Barré, J., Bousserez, N., Dominguez, J. J., Garrigues, S., Inness, A., Jones, L., Kipling, Z., Letertre-Danczak, J., Parrington, M., Razinger, M., Ribas, R., Vermoote, S., Yang, X., Simmons, A., de Marcilla, J. G., and Thépaut, J.-N.: The Copernicus Atmosphere Monitoring Service: From Research to Operations, Bull. Am. Meteorol. Soc., 103, E2650 – E2668, https://doi.org/10.1175/BAMS-D-21-0314.1, 2022.

Pierce, R. B., Al-Saadi, J., Kittaka, C., Schaack, T., Lenzen, A., Bowman, K., Szykman, J., Soja, A., Ryerson, T., Thompson, A. M., Bhartia, P., and Morris, G. A.: Impacts of background ozone production on Houston and Dallas, Texas, air quality during the Second Texas Air Quality Study field mission, J. Geophys. Res., 114, https://doi.org/10.1029/2008JD011337, 2009.

Qu, Z., Henze, D. K., Capps, S. L., Wang, Y., Xu, X., Wang, J., and Keller, M.: Monthly top-down $NO_x$ emissions for China (2005–2012): A hybrid inversion method and trend analysis, J. Geophys. Res., 122, 4600–4625, https://doi.org/10.1002/2016JD025852, 2017.

710 Qu, Z., Henze, D. K., Li, C., Theys, N., Wang, Y., Wang, J., Wang, W., Han, J., Shim, C., Dickerson, R. R., and Ren, X.: SO2 Emission Estimates Using OMI SO2 Retrievals for 2005–2017, J. Geophys. Res., 124, 8336–8359, https://doi.org/10.1029/2019JD030243, 2019a.

Qu, Z., Henze, D. K., Theys, N., Wang, J., and Wang, W.: Hybrid Mass Balance/4D-Var Joint Inversion of $NO_x$ and $SO_2$ Emissions in East Asia, J. Geophys. Res., 124, 8203–8224, https://doi.org/10.1029/2018JD030240, 2019b.

Qu, Z., Henze, D. K., Cooper, O. R., and Neu, J. L.: Impacts of global $NO_x$ inversions on $NO_2$ and ozone simulations, Atmos. Chem. Phys.,
715 20, 13 109–13 130, https://doi.org/10.5194/acp-20-13109-2020, 2020.

Quesada-Ruiz, S., Attié, J.-L., Lahoz, W. A., Abida, R., Ricaud, P., El Amraoui, L., Zbinden, R., Piacentini, A., Joly, M., Eskes, H., Segers, A., Curier, L., de Haan, J., Kujanpää, J., Oude Nijhuis, A. C. P., Tamminen, J., Timmermans, R., and Veefkind, P.: Benefit of ozone observations from Sentinel-5P and future Sentinel-4 missions on tropospheric composition, Atmos. Meas. Tech., 13, 131–152, https://doi.org/10.5194/amt-13-131-2020, 2020.

720 Randerson, J., van der Werf, G., Giglio, L., Collatz, G., and Kasibhatla, P.: Global Fire Emissions Database, Version 4.1 (GFEDv4.1), https://doi.org/10.3334/ORNLDAAC/1293, ORNL DAAC, Oak Ridge, Tennessee, USA, 2018.

Remer, L. A., Kaufman, Y. J., Tanré, D., Mattoo, S., Chu, D. A., Martins, J. V., Li, R. R., and coauthors: The MODIS Aerosol Algorithm, Products, and Validation, J. Atmos. Sci., 62, 947–973, https://doi.org/10.1175/JAS3385.1, 2005.

Ryu, Y.-H. and Min, S.-K.: Long-term evaluation of atmospheric composition reanalyses from CAMS, TCR-2, and
725 MERRA-2 over South Korea: Insights into applications, implications, and limitations, Atmos. Enviro., 246, 118 062, https://doi.org/10.1016/j.atmosenv.2020.118062, 2021.

Schaack, T. K., Zapotocny, T. H., Lenzen, A. J., and Johnson, D. R.: Global Climate Simulation with the University of Wisconsin Global Hybrid Isentropic Coordinate Model, Journal of Climate, 17, 2998–3016, https://doi.org/10.1175/1520-0442(2004)017<2998:GCSWTU>2.0.CO;2, 2004.

730 Schultz, M. G., Schröder, S., Lyapina, O., Cooper, O. R., Galbally, I., Petropavlovskikh, I., von Schneidemesser, E., Tanimoto, H., Elshorbany, Y., Naja, M., Seguel, R. J., Dauert, U., Eckhardt, P., Feigenspan, S., Fiebig, M., Hjellbrekke, A.-G., Hong, Y.-D., Kjeld, P. C., Koide, H., Lear, G., Tarasick, D., Ueno, M., Wallasch, M., Baumgardner, D., Chuang, M.-T., Gillett, R., Lee, M., Molloy, S., Moolla, R., Wang, T., Sharps, K., Adame, J. A., Ancellet, G., Apadula, F., Artaxo, P., Barlasina, M. E., Bogucka, M., Bonasoni, P., Chang, L., Colomb, A., Cuevas-Agulló, E., Cupeiro, M., Degorska, A., Ding, A., Fröhlich, M., Frolova, M., Gadhavi, H., Gheusi, F., Gilge, S., Gonzalez, M. Y.,
735 Gros, V., Hamad, S. H., Helmig, D., Henriques, D., Hermansen, O., Holla, R., Hueber, J., Im, U., Jaffe, D. A., Komala, N., Kubistin, D., Lam, K.-S., Laurila, T., Lee, H., Levy, I., Mazzoleni, C., Mazzoleni, L. R., McClure-Begley, A., Mohamad, M., Murovec, M., Navarro-Comas, M., Nicodim, F., Parrish, D., Read, K. A., Reid, N., Ries, L., Saxena, P., Schwab, J. J., Scorgie, Y., Senik, I., Simmonds, P., Sinha, V., Skorokhod, A. I., Spain, G., Spangl, W., Spoor, R., Springston, S. R., Steer, K., Steinbacher, M., Suharguniyawan, E., Torre, P., Trickl, T., Weili, L., Weller, R., Xiaobin, X., Xue, L., and Zhiqiang, M.: Tropospheric Ozone Assessment Report: Database and metrics data of
740 global surface ozone observations, Elem. Sci. Anth., 5, 58, https://doi.org/10.1525/elementa.244, 2017.

Sekiya, T., Miyazaki, K., Ogochi, K., Sudo, K., and Takigawa, M.: Global high-resolution simulations of tropospheric nitrogen dioxide using CHASER V4.0, Geosci. Model Dev., 11, 959–988, https://doi.org/10.5194/gmd-11-959-2018, 2018.

Sekiya, T., Kanaya, Y., Sudo, K., Taketani, F., Iwamoto, Y., Aita, M. N., Yamamoto, A., and Kawamoto, K.: Global Bromine- and Iodine-Mediated Tropospheric Ozone Loss Estimated Using the CHASER Chemical Transport Model, SOLA, 16, 220–227,
745 https://doi.org/10.2151/sola.2020-037, 2020.

Sekiya, T., Miyazaki, K., Eskes, H., Sudo, K., Takigawa, M., and Kanaya, Y.: A comparison of the impact of TROPOMI and OMI tropospheric NO$_2$ on global chemical data assimilation, Atmos. Meas. Tech., 15, 1703–1728, https://doi.org/10.5194/amt-15-1703-2022, 2022.

Sherwen, T., Schmidt, J. A., Evans, M. J., Carpenter, L. J., Großmann, K., Eastham, S. D., Jacob, D. J., Dix, B., Koenig, T. K., Sinreich, R.,
Ortega, I., Volkamer, R., Saiz-Lopez, A., Prados-Roman, C., Mahajan, A. S., and Ordóñez, C.: Global impacts of tropospheric halogens
750    (Cl, Br, I) on oxidants and composition in GEOS-Chem, Atmos. Chem. Phys., 16, 12 239–12 271, https://doi.org/10.5194/acp-16-12239-2016, 2016.

Shu, L., Zhu, L., Bak, J., Zoogman, P., Han, H., Liu, S., Li, X., Sun, S., Li, J., Chen, Y., Pu, D., Zuo, X., Fu, W., Yang, X., and Fu, T.-M.: Improving ozone simulations in Asia via multisource data assimilation: results from an observing system simulation experiment with GEMS geostationary satellite observations, Atmos. Chem. Phys., 23, 3731–3748, https://doi.org/10.5194/acp-23-3731-2023, 2023.

755 Sindelarova, K., Granier, C., Bouarar, I., Guenther, A., Tilmes, S., Stavrakou, T., Müller, J.-F., Kuhn, U., Stefani, P., and Knorr, W.: Global data set of biogenic VOC emissions calculated by the MEGAN model over the last 30 years, Atmos. Chem. Phys., 14, 9317–9341, https://doi.org/10.5194/acp-14-9317-2014, 2014.

Skachko, S., Errera, Q., Ménard, R., Christophe, Y., and Chabrillat, S.: Comparison of the ensemble Kalman filter and 4D-Var assimilation methods using a stratospheric tracer transport model, Geosci. Model Dev., 7, 1451–1465, https://doi.org/10.5194/gmd-7-1451-2014, 2014.

760 Smit, H. G. J., Straeter, W., Johnson, B. J., Oltmans, S. J., Davies, J., Tarasick, D. W., Hoegger, B., Stubi, R., Schmidlin, F. J., Northam, T.,
Thompson, A. M., Witte, J. C., Boyd, I., and Posny, F.: Assessment of the performance of ECC-ozonesondes under quasi-flight conditions in the environmental simulation chamber: Insights from the Juelich Ozone Sonde Intercomparison Experiment (JOSIE), J. Geophys. Res., 112, https://doi.org/10.1029/2006JD007308, 2007.

Soja, A. J., Cofer, W. R., Shugart, H. H., Sukhinin, A. I., Stackhouse Jr., P. W., McRae, D. J., and Conard, S. G.: Estimating fire emissions
765 and disparities in boreal Siberia (1998–2002), J. Geophys. Res, 109, https://doi.org/10.1029/2004JD004570, 2004.

Stein, O., Schultz, M. G., Bouarar, I., Clark, H., Huijnen, V., Gaudel, A., George, M., and Clerbaux, C.: On the wintertime low bias of Northern Hemisphere carbon monoxide found in global model simulations, Atmos. Chem. Phys., 14, 9295–9316, https://doi.org/10.5194/acp-14-9295-2014, 2014.

Szopa, S., Naik, V., Adhikary, B., Artaxo, P., Berntsen, T., Collins, W., Fuzzi, S., Gallardo, L., Kiendler-Scharr, A., Klimont, Z., Liao, H.,
770 Unger, N., and Zanis, P.: Short-Lived Climate Forcers, in: Climate Change 2021: The Physical Science Basis, edited by Masson-Delmotte,
V., Zhai, P., Pirani, A., Connors, S., C. Péan, S. B., Caud, N., Chen, Y., Goldfarb, L., Gomis, M., Huang, M., Leitzell, K., Lonnoy, E.,
Matthews, J., Maycock, T., Waterfield, T., Yelekçi, O., Yu, R., and Zhou, B., pp. 817–922, Cambridge University Press, Cambridge, United
Kingdom and New York, NY, USA, https://doi.org/10.1017/9781009157896.008, 2021.

Tarasick, D., Galbally, I. E., Cooper, O. R., Schultz, M. G., Ancellet, G., Leblanc, T., Wallington, T. J., Ziemke, J., Liu, X., Steinbacher, M.,
775 Staehelin, J., Vigouroux, C., Hannigan, J. W., García, O., Foret, G., Zanis, P., Weatherhead, E., Petropavlovskikh, I., Worden, H., Osman,
M., Liu, J., Chang, K.-L., Gaudel, A., Lin, M., Granados-Muñoz, M., Thompson, A. M., Oltmans, S. J., Cuesta, J., Dufour, G., Thouret, V.,
Hassler, B., Trickl, T., and Neu, J. L.: Tropospheric Ozone Assessment Report: Tropospheric ozone from 1877 to 2016, observed levels,
trends and uncertainties, Elem. Sci. Anth., 7, 39, https://doi.org/10.1525/elementa.376, 2019.

Timmermans, R., Segers, A., Curier, L., Abida, R., Attié, J.-L., El Amraoui, L., Eskes, H., de Haan, J., Kujanpää, J., Lahoz, W., Oude Nijhuis,
780 A., Quesada-Ruiz, S., Ricaud, P., Veefkind, P., and Schaap, M.: Impact of synthetic space-borne NO$_2$ observations from the Sentinel-4
and Sentinel-5P missions on tropospheric NO$_2$ analyses, Atmos. Chem. Phys., 19, 12 811–12 833, https://doi.org/10.5194/acp-19-12811-2019, 2019.

Travis, K. R., Jacob, D. J., Fisher, J. A., Kim, P. S., Marais, E. A., Zhu, L., Yu, K., Miller, C. C., Yantosca, R. M., Sulprizio, M. P., Thompson, A. M., Wennberg, P. O., Crounse, J. D., St. Clair, J. M., Cohen, R. C., Laughner, J. L., Dibb, J. E., Hall, S. R., Ullmann, K., Wolfe, G. M., Pollack, I. B., Peischl, J., Neuman, J. A., and Zhou, X.: Why do models overestimate surface ozone in the Southeast United States?, Atmos. Chem. Phys., 16, 13 561–13 577, https://doi.org/10.5194/acp-16-13561-2016, 2016.

Turnock, S. T., Allen, R. J., Andrews, M., Bauer, S. E., Deushi, M., Emmons, L., Good, P., Horowitz, L., John, J. G., Michou, M., Nabat, P., Naik, V., Neubauer, D., O'Connor, F. M., Olivié, D., Oshima, N., Schulz, M., Sellar, A., Shim, S., Takemura, T., Tilmes, S., Tsigaridis, K., Wu, T., and Zhang, J.: Historical and future changes in air pollutants from CMIP6 models, Atmos. Chem. Phys., 20, 14 547–14 579, https://doi.org/10.5194/acp-20-14547-2020, 2020.

Veefkind, J., Aben, I., McMullan, K., Förster, H., de Vries, J., Otter, G., Claas, J., Eskes, H., de Haan, J., Kleipool, Q., van Weele, M., Hasekamp, O., Hoogeveen, R., Landgraf, J., Snel, R., Tol, P., Ingmann, P., Voors, R., Kruizinga, B., Vink, R., Visser, H., and Levelt, P.: TROPOMI on the ESA Sentinel-5 Precursor: A GMES mission for global observations of the atmospheric composition for climate, air quality and ozone layer applications, Remote Sens. Environ., 120, 70–83, https://doi.org/10.1016/j.rse.2011.09.027, 2012.

Wagner, A., Bennouna, Y., Blechschmidt, A.-M., Brasseur, G., Chabrillat, S., Christophe, Y., Errera, Q., Eskes, H., Flemming, J., Hansen, K. M., Inness, A., Kapsomenakis, J., Langerock, B., Richter, A., Sudarchikova, N., Thouret, V., and Zerefos, C.: Comprehensive evaluation of the Copernicus Atmosphere Monitoring Service (CAMS) reanalysis against independent observations: Reactive gases, Elem. Sci. Anth., 9, 00 171, https://doi.org/10.1525/elementa.2020.00171, 2021.

Waters, J., Froidevaux, L., Harwood, R., Jarnot, R., Pickett, H., Read, W., Siegel, P., Cofield, R., Filipiak, M., Flower, D., Holden, J., Lau, G., Livesey, N., Manney, G., Pumphrey, H., Santee, M., Wu, D., Cuddy, D., Lay, R., Loo, M., Perun, V., Schwartz, M., Stek, P., Thurstans, R., Boyles, M., Chandra, K., Chavez, M., Chen, G.-S., Chudasama, B., Dodge, R., Fuller, R., Girard, M., Jiang, J., Jiang, Y., Knosp, B., LaBelle, R., Lam, J., Lee, K., Miller, D., Oswald, J., Patel, N., Pukala, D., Quintero, O., Scaff, D., Van Snyder, W., Tope, M., Wagner, P., and Walch, M.: The Earth observing system microwave limb sounder (EOS MLS) on the aura Satellite, IEEE Trans. Geosci. Remote Sens., 44, 1075–1092, https://doi.org/10.1109/TGRS.2006.873771, 2006.

Wells, K. C., Millet, D. B., Payne, V. H., Vigouroux, C., Aquino, C. A. B., De Mazière, M., de Gouw, J. A., Graus, M., Kurosu, T., Warneke, C., and Wisthaler, A.: Next-Generation Isoprene Measurements From Space: Detecting Daily Variability at High Resolution, J. Geophys. Res., 127, e2021JD036 181, https://doi.org/10.1029/2021JD036181, 2022.

Wu, L., Mallet, V., Bocquet, M., and Sportisse, B.: A comparison study of data assimilation algorithms for ozone forecasts, J. Geophys. Res., 113, https://doi.org/10.1029/2008JD009991, 2008.

Wu, W.-S., Purser, R., and Parrish, D.: Three-Dimensional Variational Analysis with Spatially Inhomogeneous Covariances, Monthly Weather Review, 130, 2905–2916, https://doi.org/10.1175/1520-0493(2002)130<2905:TDVAWS>2.0.CO;2, 2002.

Yarwood, G., Rao, S., Yocke, M., and Whitten, G.: Updates to the carbon bond chemical mechanism: CB05, Final report to the US EPA, RT-0400675, 8, 13, 2005.

Young, P. J., Naik, V., Fiore, A. M., Gaudel, A., Guo, J., Lin, M. Y., Neu, J. L., Parrish, D. D., Rieder, H. E., Schnell, J. L., Tilmes, S., Wild, O., Zhang, L., Ziemke, J., Brandt, J., Delcloo, A., Doherty, R. M., Geels, C., Hegglin, M. I., Hu, L., Im, U., Kumar, R., Luhar, A., Murray, L., Plummer, D., Rodriguez, J., Saiz-Lopez, A., Schultz, M. G., Woodhouse, M. T., and Zeng, G.: Tropospheric Ozone Assessment Report: Assessment of global-scale model performance for global and regional ozone distributions, variability, and trends, Elem. Sci. Anth., 6, 10, https://doi.org/10.1525/elementa.265, 2018.

Yurganov, L. N., McMillan, W. W., Dzhola, A. V., Grechko, E. I., Jones, N. B., and van der Werf, G. R.: Global AIRS and MO-
820    PITT CO Measurements: Validation, Comparison, and Links to Biomass Burning Variations and Carbon Cycle, J. Geophys. Res, 113,
https://doi.org/10.1029/2007JD009229, 2008.

Zhang, X., Jones, D. B. A., Keller, M., Walker, T. W., Jiang, Z., Henze, D. K., Worden, H. M., Bourassa, A. E., Degenstein, D. A., and
Rochon, Y. J.: Quantifying Emissions of CO and $NO_x$ Using Observations From MOPITT, OMI, TES, and OSIRIS, J. Geophys. Res.,
124, 1170–1193, https://doi.org/10.1029/2018JD028670, 2019.

825    Zhu, C., Byrd, R. H., Lu, P., and Nocedal, J.: L-BFGS-B: A limited memory FORTRAN code for solving bound constrained
optimization problems, Tech. Rep. Tech. Rep. No. NAM-11, EECS Dept., Northwestern Univ., Evanston, Ill, available at:
http://users.iems.northwestern.edu/ nocedal/PDFfiles/lbfgsb.pdf (last access: 2 November 2020), 1994.

Ziemke, J. R., Chandra, S., Duncan, B. N., Froidevaux, L., Bhartia, P. K., Levelt, P. F., and Waters, J. W.: Tropospheric ozone determined
from Aura OMI and MLS: Evaluation of measurements and comparison with the Global Modeling Initiative's Chemical Transport Model,
830    J. Geophys. Res., 111, https://doi.org/10.1029/2006JD007089, 2006.

Ziemke, J. R., Oman, L. D., Strode, S. A., Douglass, A. R., Olsen, M. A., McPeters, R. D., Bhartia, P. K., Froidevaux, L., Labow, G. J.,
Witte, J. C., Thompson, A. M., Haffner, D. P., Kramarova, N. A., Frith, S. M., Huang, L.-K., Jaross, G. R., Seftor, C. J., Deland, M. T., and
Taylor, S. L.: Trends in global tropospheric ozone inferred from a composite record of TOMS/OMI/MLS/OMPS satellite measurements
and the MERRA-2 GMI simulation, Atmos. Chem. Phys., 19, 3257–3269, https://doi.org/10.5194/acp-19-3257-2019, 2019.

835    Zoogman, P., Jacob, D. J., Chance, K., Liu, X., Lin, M., Fiore, A., and Travis, K.: Monitoring high-ozone events in the US Intermountain
West using TEMPO geostationary satellite observations, Atmos. Chem. Phys., 14, 6261–6271, https://doi.org/10.5194/acp-14-6261-2014,
2014.
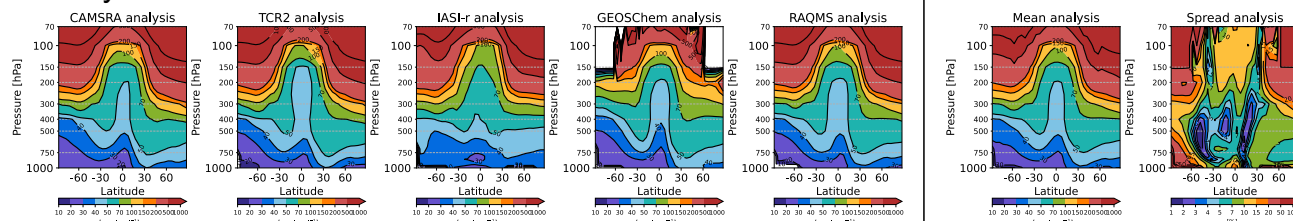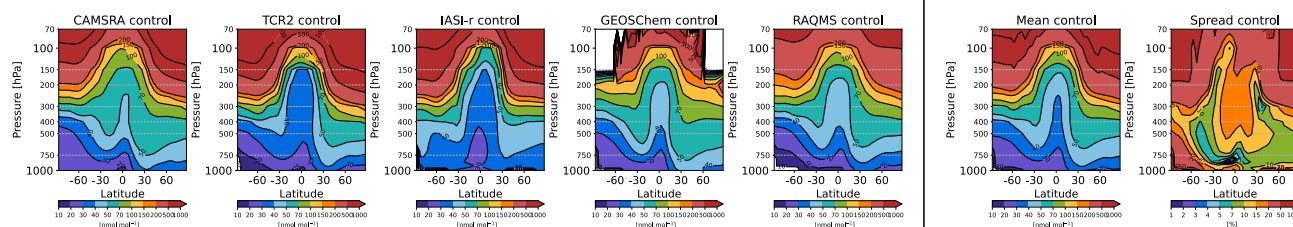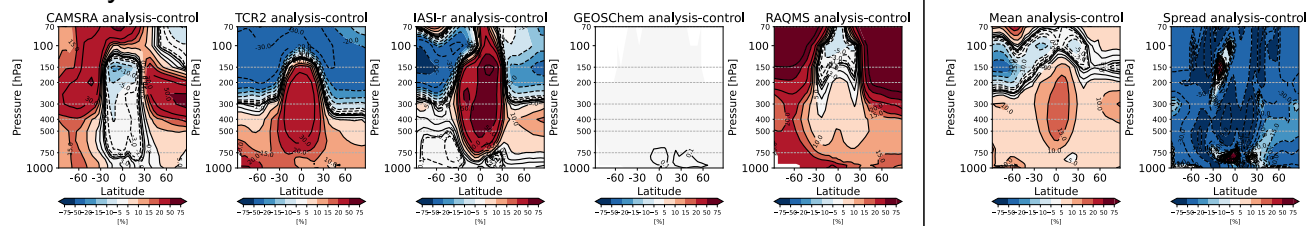
**Figure 1.** Latitude-pressure level cross sections of annual mean tropospheric ozone concentrations obtained from reanalysis products (top), control simulations (middle), and their differences (bottom) in 2010. The first through fifth columns present data from CAMSRA, TCR-2, IASI-r (MOCAGE), GEOS-Chem-adjoint, and RAQMS Aura reanalysis, and the sixth and seventh columns present multi-system average and spread normalized by the mean-system average data, respectively. The difference in the multi-system spread is defined as (stdev(reanalysis) - stdev(control)) / stdev(control) × 100, where stdev represents standard deviation. The units of ozone concentrations and the differences between reanalysis products and control simulations are mole fraction in air (nmol mol$^{-1}$) and percentage (%), respectively. The unit of multi-system spread is percentage (%).
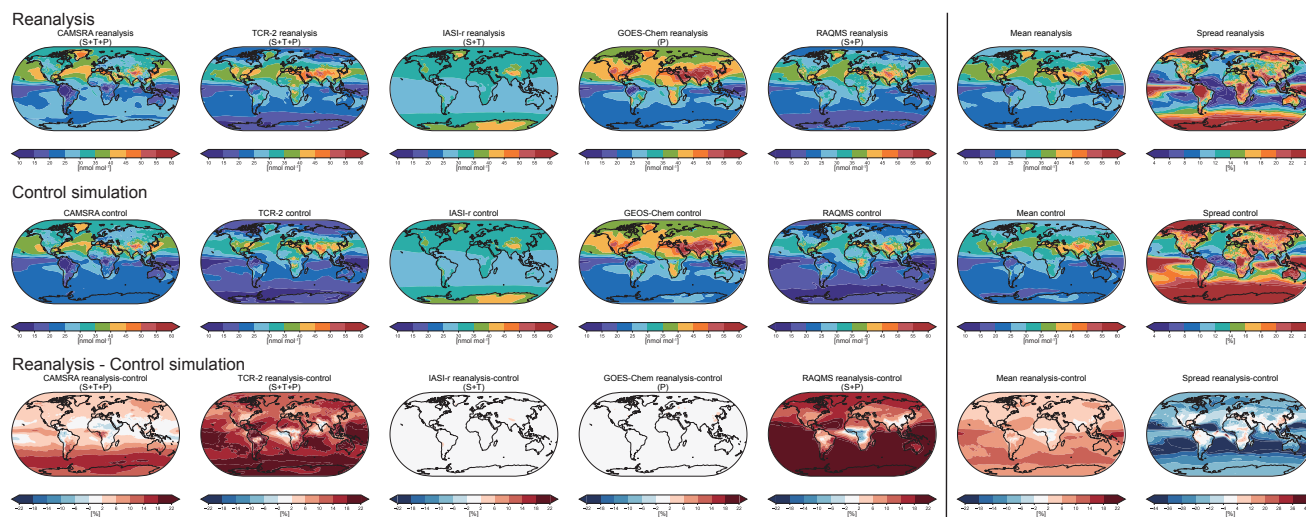
**Figure 2.** Global distribution of annual mean surface ozone concentrations obtained from the reanalysis products (top), control simulations (middle), and their differences (bottom) in 2010. The first through fifth columns represent data from CAMSRA, TCR-2, IASI-r, GEOS-Chem-adjoint, and RAQMS Aura reanalysis, and the sixth and seventh columns present multi-system average and spread normalized by the mean-system average data, respectively. The difference in the multi-system spread is defined as (stdev(reanalysis) - stdev(control)) / stdev(control) × 100, where stdev represents standard deviation. The units of ozone concentrations and the differences between reanalysis products and control simulations are mole fraction in air (nmol mol$^{-1}$) and percentage (%), respectively. The unit of multi-system spread is percentage (%).
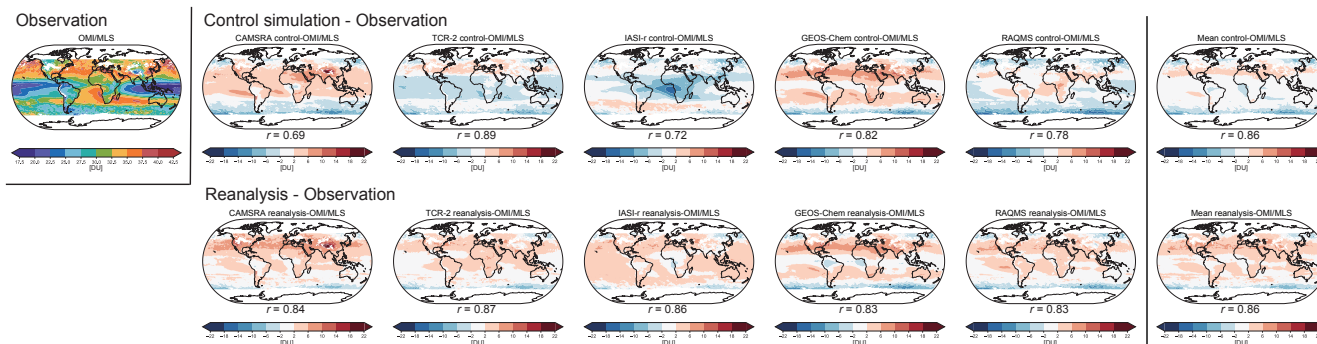
**Figure 3.** Global distributions of tropospheric ozone column (TOC) derived from the OMI-MLS observations (first column) and mean bias of the CAMSRA (second column), TCR-2 (third column), IASI-r (fourth column), the GEOS-Chem-adjoint (fifth column), the RAQMS Aura reanalysis (sixth column), and multi-system mean bias (seventh column) relative to OMI-MLS. Top and bottom panels are the control simulations and reanalysis products, respectively. The unit is the Dobuson unit (DU). The spatial correlation coefficient ($r$) between OMI-MLS and the reanalysis/control simulation is also shown below the map.
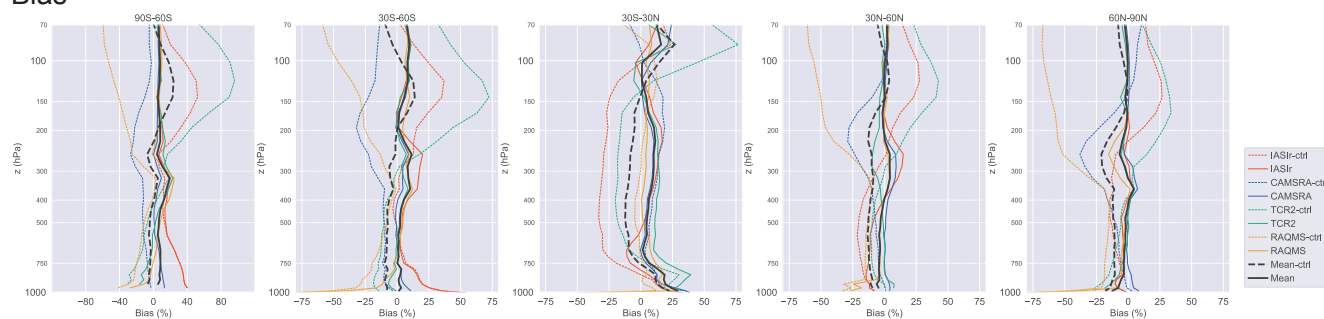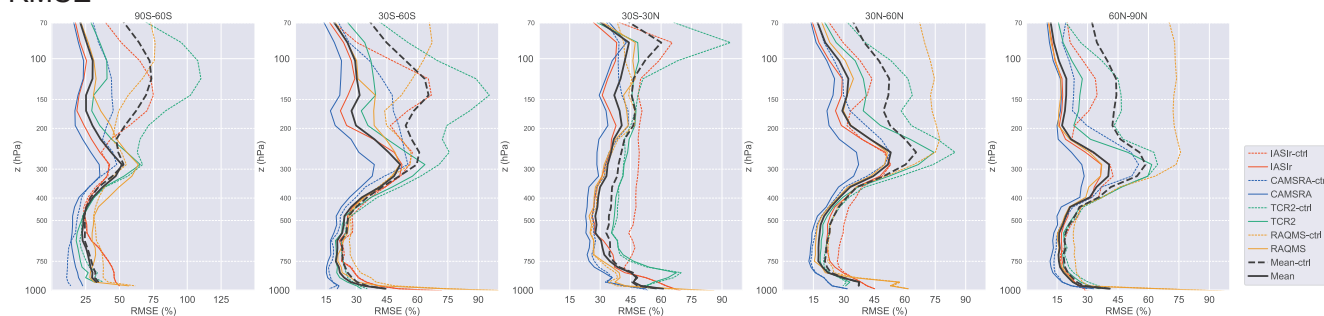
**Figure 4.** Vertical profiles of bias (top) and RMSE (bottom) for the reanalysis products and the control simulations compared to ozonesonde observations in 2010. The first through fifth columns present the southern high latitudes (60–90°S), the southern mid-latitudes (30–60°S), the tropics (30°S–30°N), the northern mid-latitudes (30–60°N), and the northern high latitudes (60–90°N). The blue line indicates CAMSRA, the red line indicates IASI-r, the green line indicates TCR-2, the orange line indicates the RAQMS Aura reanalysis, and the black line indicates multi-system averages. The solid and dashed lines indicate the reanalysis products and the control simulations, respectively. The unit is percentage (%).
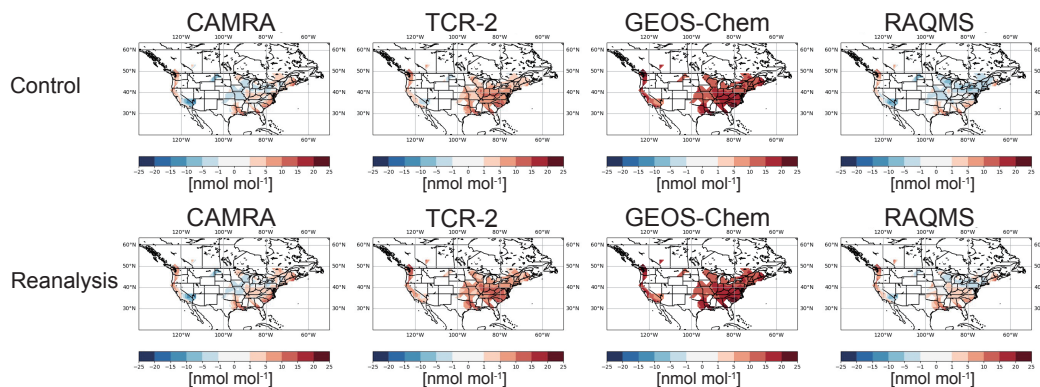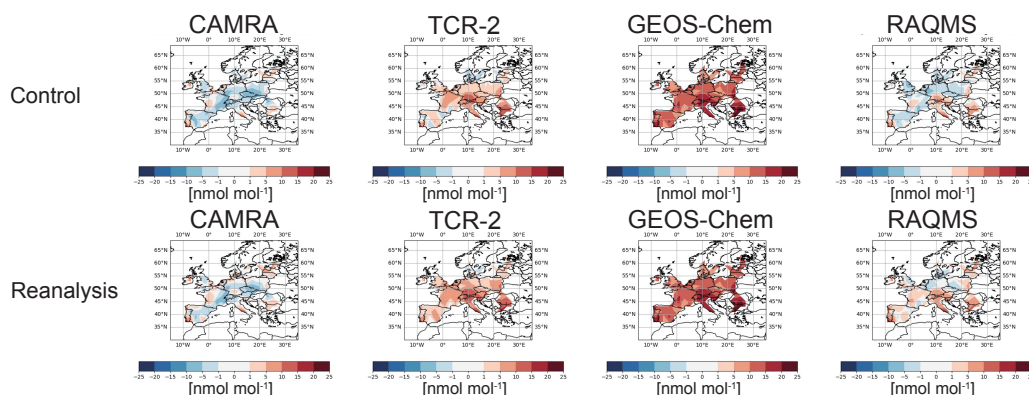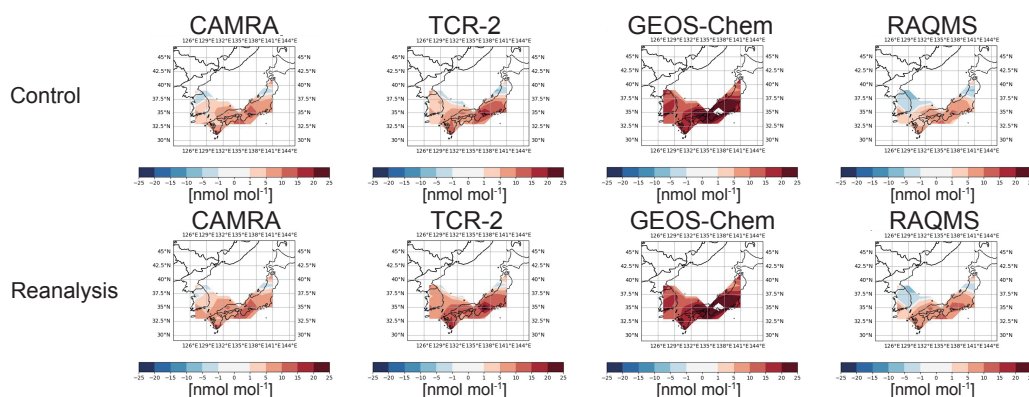
**Figure 5.** Bias of annual mean surface ozone relative to the TOAR database (nmol mol$^{-1}$) in CAMSRA (first column), TCR-2 (second column), GEOS-Chem-adjoint (third column), and the RAQMS Aura reanalysis (fourth column) in 2010. The first, third, and fifth rows are the control simulations without data assimilation, and the second, fourth, and sixth rows are the reanalysis products. The "rural_mean" aggregated data were used for the comparison. The model and reanalysis output was mapped onto the $2° \times 2°$ grid.

## Direct ozone assimilatoin (S or T)
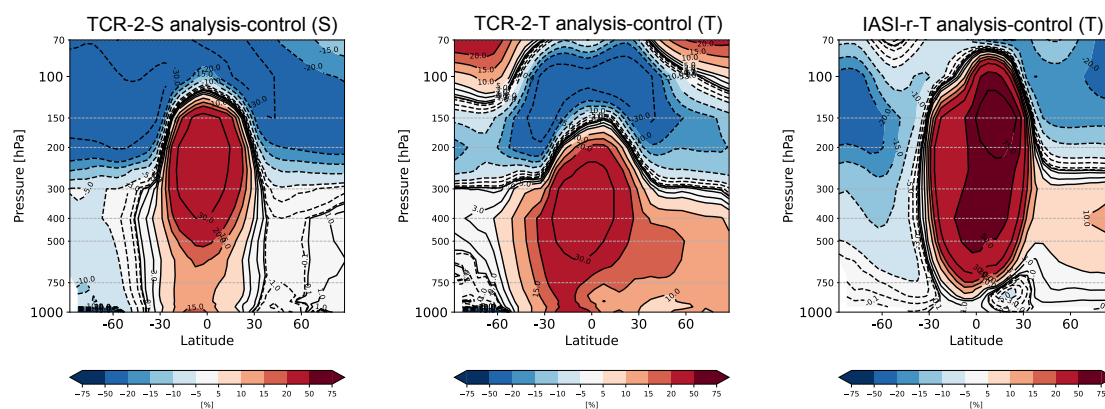
## Ozone precursor assimilatoin (P)
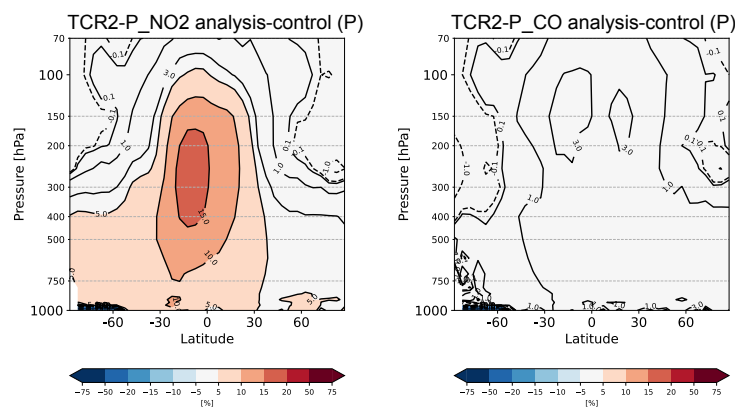
**Figure 6.** Latitude-pressure level cross sections of changes in annual mean ozone concentrations owing to data assimilation obtained from the OSEs in 2010. The top row presents the direct ozone assimilation (S and T): TCR-2-S (left), TCR-2-T (center), and IASI-r-T (right); and the bottom row presents the assimilation of ozone precursors (P): TCR-2-P_NO$_x$ (left), and TCR-2-P_CO (center). The units are percentage (%).
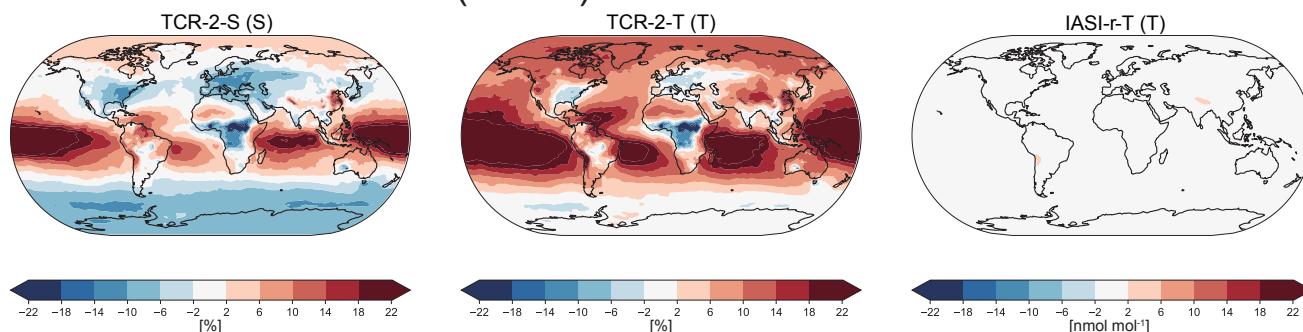
**Figure 7.** Global distribution of changes in annual mean surface ozone concentrations owing to data assimilation obtained from OSEs in 2010. The top row presents the direct ozone assimilation (S and T): TCR-2-S (left), TCR-2-T (center), and IASI-r-T (right); and the bottom row presents the assimilation of ozone precursors (P): TCR-2-P_NO$_x$ (left), and TCR-2-P_CO (center). The unit is percentage (%).

**Table 1.** List of chemical reanalysis systems used in this study.

| Reanalysis system | Resolution | Scheme | Assimilated observations | | | | |
|---|---|---|---|---|---|---|---|
| | | | Stratospheric ozone (S) | | Tropospheric ozone (T) | Precursor gases (P) | Reference |
| | | | Total column | Profile /Partial column | | | |
| CAMSRA | $0.75° \times 0.75°$ | 4D-Var | OMI GOME2, SCIAMACHY, TROPOMI, OMPS | SBUV, MLS, MIPAS | | MOPITT (CO), OMI (NO$_2$) | Inness et al. (2019) |
| TCR-2 | $1.1° \times 1.1°$ | EnKF | | MLS | TES | MOPITT (CO), OMI, SCIAMACHY, GOME-2 (NO$_2$) | Miyazaki et al. (2020a) |
| IASI-r | $2° \times 2°$ | 3D-Var | | MLS | IASI (L1) | | Emili and El Aabaribaoune (2021) |
| GEOS-Chem | $2° \times 2.5°$ | 4D-Var | | | | OMI (NO$_2$) | Qu et al. (2020) |
| RAQMS | $1° \times 1°$ | 3D-Var | OMI | MLS | | AIRS (CO), OMI (NO$_2$) | Pierce et al. (2009) |
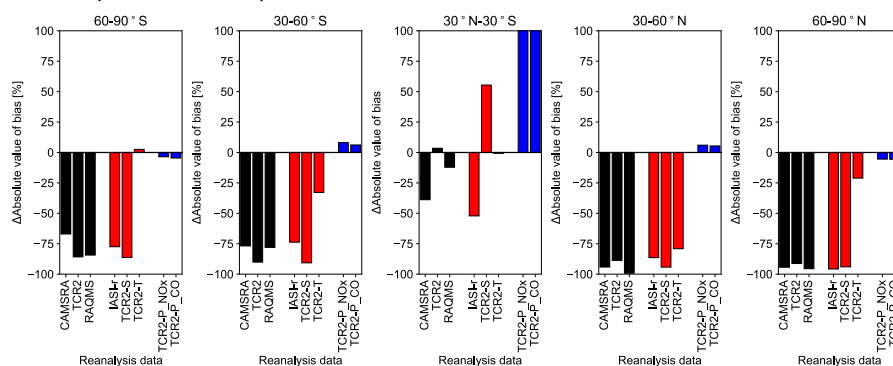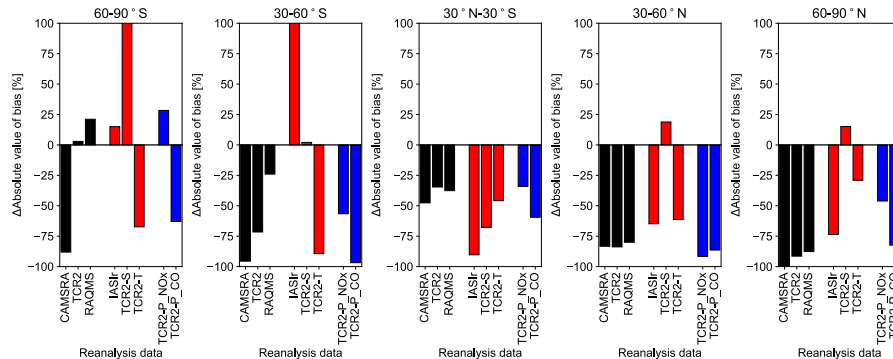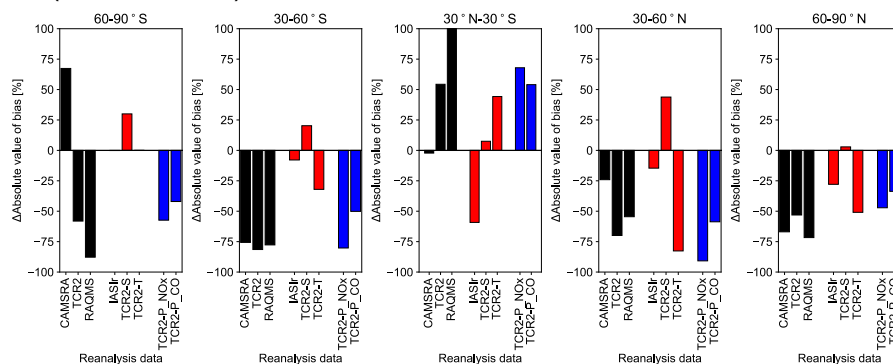
**Figure 8.** Relative changes in the absolute value of the mean bias (%) due to data assimilation in the reanalysis products and OSEs. These changes are calculated as follows: $(|\mathrm{MB_{DA}}| - |\mathrm{MB_{CTL}}|)\,/\,|\mathrm{MB_{CTL}}| \times 100$, where MB is mean bias. Upper row is the upper troposphere and lower stratosphere (UTLS, 70–250 hPa), middle row is the middle troposphere (MT, 400–600 hPa), and bottom row is the lower troposphere (LT, 800–900 hPa) in 2010. First through fifth columns present the southern high latitudes (60–90°S), the southern mid latitudes (30–60°S), the tropics (30°N–30°S), the northern mid latitudes (30–60°N), and the north high latitudes (60–90°N). The black bars indicate the simultaneous assimilation of ozone and its precursors (S+T+P and S+P): CAMSRA, TCR-2, and the RAQMS Aura reanalysis. The red bars indicate the direct ozone assimilation (S+T, S, and T): IASI-r, TCR-2-S, and TCR-2-T, and the blue bars indicate the assimilation of ozone precursors (P): TCR-2-P_NO$_x$ and TCR-2-P_CO.
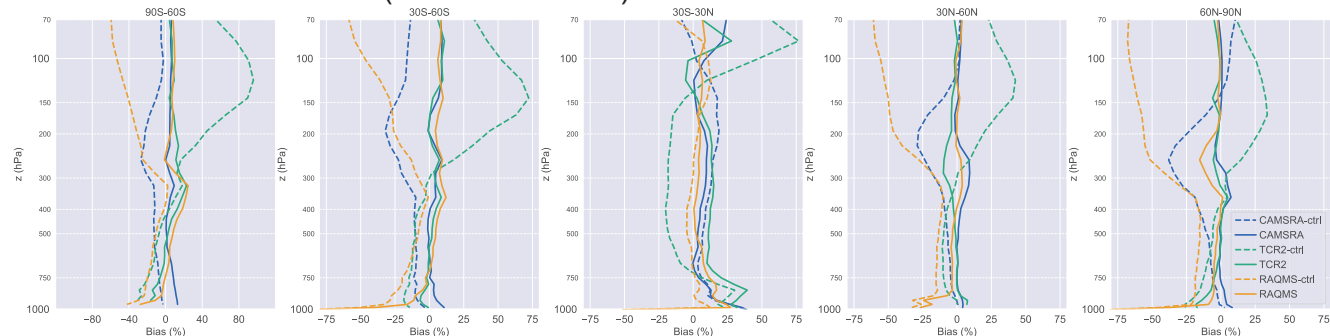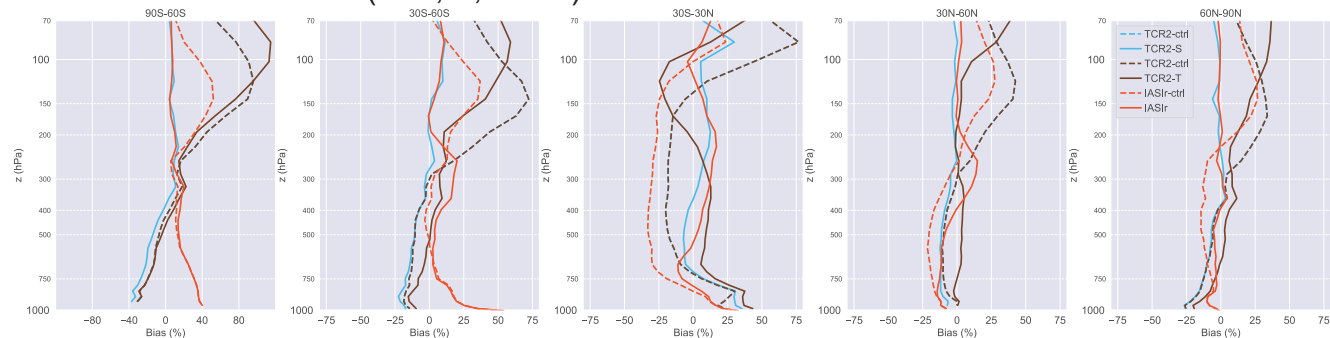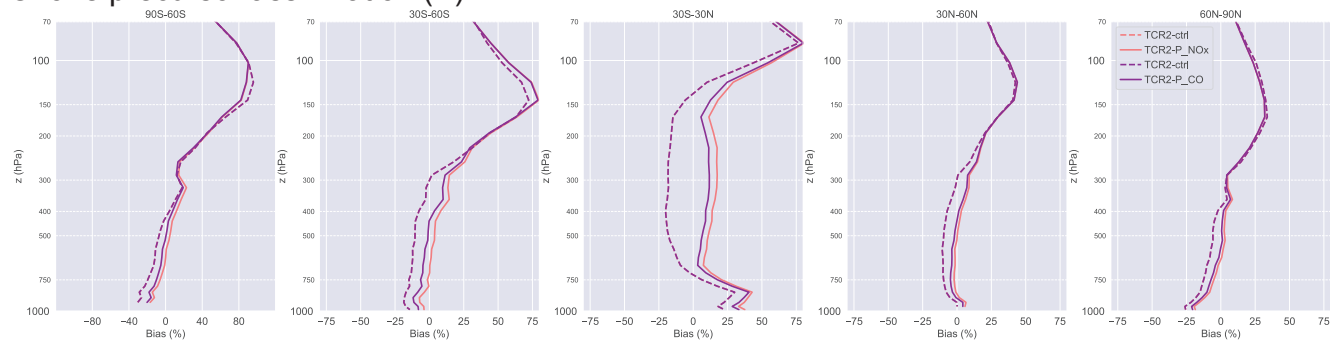
**Figure 9.** Vertical profiles of the bias for the data assimilation (solid lines) and the control simulations (dashed lines) relative to ozonesonde observations in 2010. Top panels are the simultaneous assimilation (S+T+P and S+P), middle panels are the direct ozone assimilation (S+T, S, and T), and bottom panels are the ozone precursors assimilation (P). First through fifth columns present the southern high latitudes (60–90°S), the southern mid-latitudes (30–60°S), the tropics (30°S–30°N), the northern mid-latitudes (30–60°N), and the northern high latitudes (60–90°N). The blue line indicates CAMSRA, the green line indicates TCR-2, the orange line indicates the RAQMS Aura reanalysis, the red line indicates IASI-r, the sky-bule line indicates TCR-2-S, the brown line is TCR-2-T, the pink line is TCR-2-P_NO$_x$, and the purple line indicates TCR-2-P_CO. The unit is percentage (%).

**Table 2.** List of experiments used in this study. S, T, and P represent the assimilation of satellite observations of stratospheric and tropospheric ozone and its precursors, respectively). CTL represents the control simulations without any data assimilation. $X^F$ denotes the assimilation of full set of observations for each system.

| | Ozone+Precursor | | Ozone | | | Precursor | | |
|---|---|---|---|---|---|---|---|---|
| Reanalysis | S+T+P | S+P | S+T | S | T | P(NO$_2$) | P(CO) | CTL |
| CAMSRA | | $X^F$ | | | | | | X |
| TCR-2 | $X^F$ | | | X | X | X | X | X |
| IASI-r | | | $X^F$ | | X | | | X |
| GEOS-Chem | | | | | | $X^F$ | | X |
| RAQMS | | $X^F$ | | | | | | X |

**Table 3.** Mean bias (MB) ranges between different systems and root-mean-square errors (RMSEs) multi-system mean and spread for the reanalysis [control simulation in the square brackets] against ozonesonde observations in the upper troposphere (UTLS), middle troposphere (MT), and lower troposphere (LT) over five latitude bands. The unit is percentage (%).

| | | 60–90°S | 30–60°S | 30°S–30°N | 30–60°N | 60–90°N | Global |
|---|---|---|---|---|---|---|---|
| UTLS (70–250 hPa) | MB | 5–9 [-40–64] | 5–7 [-32–49] | 6–8 [-16–12] | -3–2 [-48–28] | -3–(-0.6) [-59–26] | -1–2 [-47–30] |
| | RMSE | 31±8 [62±17] | 30±6 [57±12] | 40±5 [48±6] | 31±7 [52±16] | 18±4 [44±18] | 30±7 [55±17] |
| MT (400–600 hPa) | MB | 1–15 [-12–13] | -0.5–6 [-10–(-2)] | 2–12 [-32–8] | -7–1 [-20–(-8)] | -4–0.4 [-16–(-5)] | -3–1 [-18–(-6)] |
| | RMSE | 25±6 [25±4] | 27±3 [28±3] | 28±5 [34±8] | 22±2 [26±4] | 21±3 [25±2] | 23±3 [28±4] |
| LT (800–900 hPa) | MB | -3–34 [-24–34] | -3–13 [-22–14] | 2–31 [-5–20] | -14–3 [-17–(-3)] | -7–1 [-19–(-4)] | -7–3 [-14–(-2)] |
| | RMSE | 29±10 [31±12] | 22±5 [25±5] | 42±10 [43±10] | 22±4 [24±5] | 18±3 [20±4] | 25±5 [27±5] |